MASTER'S DEGREE THESIS

MSc in Applied Mathematics

Title: Virtual orbits and two-parameter bifurcation analysis in power electronic converters

Author: Albert Granados Corsellas

Advisor: Enric Fossas Colet

Department: Enginyeria de Sistemes, Automàtica i Informàtica Industrial

Academic year: 2008/2009

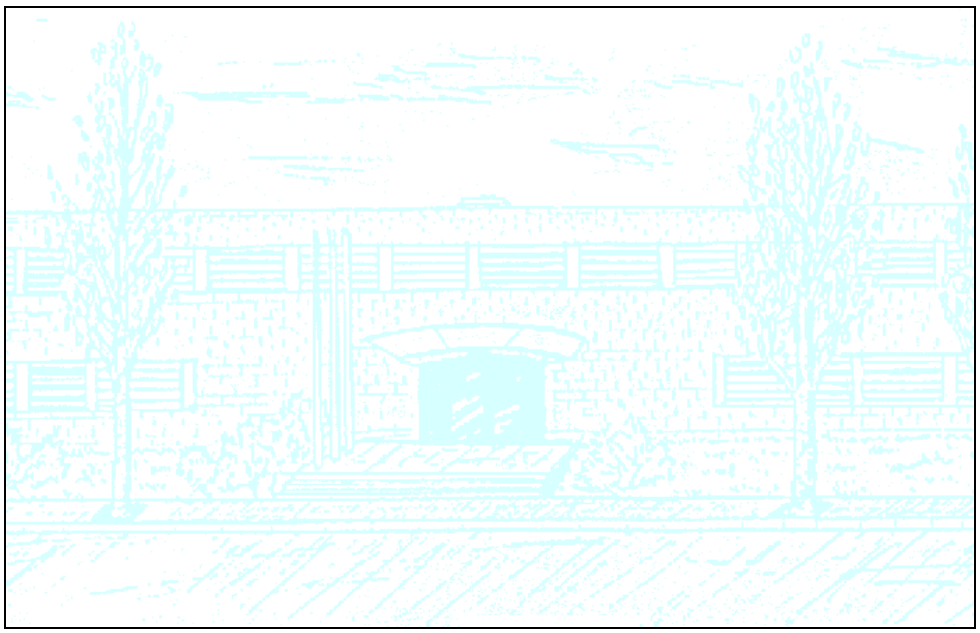

Facultat de Matemàtiques i Estadística

UNIVERSITAT POLITÈCNICA DE CATALUNYA

Summary

When analytically investigating the 2-parameter bifurcation behaviour on a buck converter controlled by the ZAD strategy, the period doubling and corner collision curves in parameter space presented in [1] cross in four codimension two points presenting several properties. While two of them are given by the destruction of two bifurcation curves (period doubling and corner collision) at the boundaries of the feasible region in parameter space, a third one represents a change on the dynamics of the system and the fourth one is given by "appearance" of a saddle-node bifurcation curve.
Using the concept of virtual and feasible orbits in the state space we will explain in this work how exactly this curve "appears" and we will add a fifth codimension two point where this saddle node bifurcation is destroyed and the corresponding curve "disappears". We will also explain which are the changes on the dynamics of the system involved on the third codimension two point and we will give a partition of the parameter space so indicating where saturated and unsaturated T and $2T$-periodic orbits exist.
On the other hand, adding a third parameter representing a perturbation on the ZAD condition in one iteration of two periodic orbits, we will analytically show how some of the obtained phenomena are not possible to observe numerically due to the destruction of some of the previous structures for arbitrary small values of this parameter. At the same time, we will also justify why the numerical results when using an approximation of the ZAD condition (see [3]) contradict the analytical ones shown in [1].

Contents

Chapter 1

Introduction

Nowadays, due to the increasing use of mobile electronic devices and to the avoiding fuel tendency, the use of batteries is being more and more extended. Energy saving demands not only higher efficiency in these power supply devices but also a more accurate control on the conversion of the voltage obtained from the battery and the one requested by the electronic device. This conversion is achieved by a DC/DC power electronic converter applying two different circuits during a certain time and repeats this operation in a high frequency manner. The key aspect on the control of this device and therefore the guaranty of the desired voltage is the design of a *duty cycle* which determines these certain times and, in the most sophisticated cases, is allowed to vary with the system variables (normally a current and a voltage).
The switching behaviour of this converter leads to a model which is piecewise continuous on the right hand (also called Filippov systems), and the repeating behaviour makes the system non-autonomous but periodic. This property permits the use of averaging methods for the control design, such as working with the averaged system (see for instance [11]) or the use of the so-called ZAD strategy (zero average dynamics).
In this work we consider a DC/DC buck converter controlled by a law based on the ZAD strategy leading the control design to the choice of a certain constant. This parameter together with the (constant) desired voltage define a two dimensional parameter space exhibiting not only phenomena typical from smooth systems as period doubling bifurcations but also corner collision bifurcations which are unique of nonsmooth systems. These strange behaviours have converted these kind of systems into an important center of study leading many authors to investigate them often using the buck converter as one of the principle examples (see for instance Di Bernardo *et al.* [5] for a comprehensive account of the latest developments in this field).
Recent studies on the two-parameter bifurcation analysis on the ZAD con-

trolled buck converter show that this parameter space contents a rich and complex structure ([1, 2, 3]); moreover, the use of a linear approximation of the ZAD condition ([3]) entails qualitative differences with the analytical ones ([1]) so motivating the main sense of our work. This is organized as follows.

Chapter 2 consists on an introduction to the system and to the ZAD condition. In Chapter 3 we give a brief review to the previous results distinguishing between the use of numeric and analytics. In Chapter 4 we introduce the concept of virtual and feasible orbits in order to go deeper on the two-parameter bifurcation analysis. The saddle-node bifurcation curve is given together with a new codimension two point and we show how these objects play an important role on the existence of saturated 2-periodic orbits. We also show how numerical simulations do not hold the analytics even avoiding the use of the linear approximation. Finally, in Chapter 5, we analytically investigate a perturbation on the ZAD condition in one iteration of 2-periodic orbits, permitting us to give a possible explanation to these differences.

Chapter 2

System description and previous tools

2.1 Introduction

Let us consider the power converter which scheme is shown in Figure 2.1. This kind of device is called a DC/DC Buck converter as it reduces a certain input voltage E to another certain voltage v_{o}, which is desired to follow a reference signal v_{ref}, which can be constant or not.
As one can see in Figure 2.1, the circuit is regulated by a PWM (Pulse Width Modulator) block which commutes the system between two different topologies, shown in Figure 2.2. System is in topology A (Figure 2.2(a)) during a certain time $T_{\mathrm{on}} = d \cdot T$, while it is in topology B during $T_{\mathrm{off}} = (1-d) \cdot T$ seconds. This is repeated every T seconds so, if parameter d is constant, then the system has a periodic behaviour. In any case, parameter d will always be considered to be constant at each period and will only be allowed to change at the beginning of each sampling period T.
Besides the values of the inductor (L), capacitor (C) and resistor (R), the key on the control design in order to make v_{o} follow the reference signal v_{ref}, is the value of parameter d. There exists many ways to design a control action to solve this tracking or regulating problem. The one we are going to consider here is proposed by Fossas *et al.* [2]. It is called ZAD (Zero Average Dynamics) and its goal is the zero average fulfillment of the difference between the output v_o and the desired voltage v_{ref} and their derivatives on each T-period.

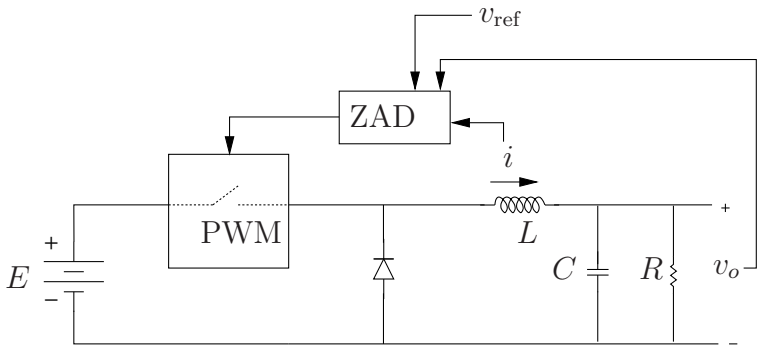

Figure 2.1: Buck Converter.

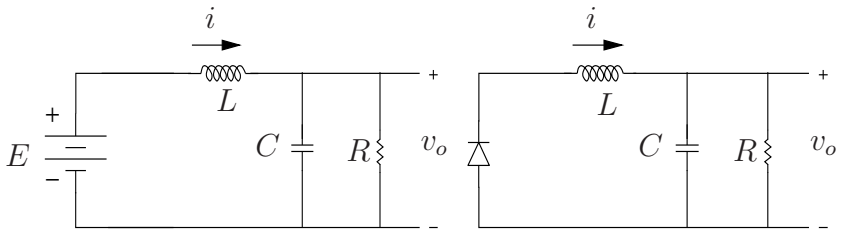

(a) Topology A (b) Topology B

Figure 2.2: Switching topologies for the buck converter.

2.2 System equations

Let i and v_0 be the current on the inductor and the voltage on the capacitor, also the output voltage, respectively. Taking these two magnitudes as state variables, the differential equations that model the system behaviour can be written as

$$\begin{cases} \dfrac{dv_o}{dt} = \dfrac{1}{C}\left(i - \dfrac{v_o}{R}\right) \\ \\ \dfrac{di}{dt} = \dfrac{1}{L}\left(E \cdot \tilde{u} - v_o\right) \end{cases}, \tag{2.1}$$

where, d_k is the value of the duty cycle in the current sampling period kT and $\tilde{u}$ is the control function defined as

$$\tilde{u} = \begin{cases} 1, & kT \leq t \leq kT + Td_k/2 \\ 0, & kT + Td_k/2 \leq t \leq (k+1)T - Td_k/2 \\ 1, & (k+1)T - Td_k/2 \leq t \leq (k+1)T \end{cases}, \tag{2.2}$$

modeling a central PWM. Notice that $d_k \in [0, 1]$ and that $d_k = 0$ corresponds to $\tilde{u} = 0$ and $d_k = 1$ corresponds to $\tilde{u} = 1$ on $[kT, (k+1)T]$. We will say that

the system gets saturated in these last two situations.
Applying the change of variables

$$x_1 = \frac{v_o}{E},$$

$$x_2 = \sqrt{\frac{L}{C}}\frac{1}{E}i,$$

$$t = \frac{\tau}{\sqrt{LC}},$$

and recalling

$$\dot{} = \frac{d}{d\tau},\ T := \frac{T}{\sqrt{LC}},\ d := \frac{d}{\sqrt{LC}},$$

one obtains the dimensionless version of the system equations

$$\begin{cases} \dot{x}_1 = x_2 - \gamma x_1 \\ \dot{x}_2 = \tilde{u} - x_1 \end{cases}, \tag{2.3}$$

where

$$\gamma = \frac{1}{R}\sqrt{\frac{L}{C}}.$$

Calling

$$A = \begin{pmatrix} -\gamma & 1 \\ -1 & 0 \end{pmatrix},$$

system equations can also be written in matrix form as

$$\dot{x} = Ax + u, \tag{2.4}$$

where $x = (x_1, x_2)^T$,

$$u = \begin{cases} B_1, & kT \le t \le kT + Td_k/2 \\ B_2, & kT + Td_k/2 \le t \le (k+1)T - Td_k/2 \\ B_1, & (k+1)T - Td_k/2 \le t \le (k+1)T \end{cases}, \tag{2.5}$$

$$B_1 = \begin{pmatrix} 0 \\ 1 \end{pmatrix},$$

and

$$B_2 = \begin{pmatrix} 0 \\ 0 \end{pmatrix}.$$

2.3 Poincaré map

In order to cover a deeper analysis of the systems behaviour, as existence of periodic orbits or bifurcations, it is usefull to work with the Poincaré map instead of the differential equations of the system.
As system (2.4) is not autonomous but periodic, we can define the Poincaré map as the stroboscopic mapping $P(x_0) := \Phi(T, x_0)$, where $\Phi(t, x_0)$ is the flow of the system (2.4) verifying $\Phi(0, x_0) = x_0$. As also system (2.4) is (piecewise)-linear, we can use that the general solution of a linear system $\dot{x} = Ax + B$ with initial condition $x(0) = x_0$ is given by

$$\Gamma(t, x_0, B) := \left(-I + e^{At}\right) A^{-1}B + e^{At}x_0 \tag{2.6}$$

and define

$$\Phi_i(t, x_0) := \Gamma(t, x_0, B_i) \tag{2.7}$$

in order to obtain the image of the Poincaré map as

$$P(x_0, d) = \Phi_1\Big(Td/2, \Phi_2\Big(T - dT, \Phi_1\big(Td/2, x_0\big)\Big)\Big). \tag{2.8}$$

Finally, substituting equations (2.6) and (2.7) in equation (2.8), we obtain

$$P(x_0, d) = e^{AT}x_0 + \left(e^{AT} - I\right) A^{-1}B_1 + \left(e^{\frac{ATd}{2}} - e^{AT\left(1 - \frac{d}{2}\right)}\right) A^{-1}B_1. \tag{2.9}$$

Once the Poincaré map is introduced, we will identify from now n-periodic orbits of this map with nT-periodic orbits of the original flow. We will also refer as *fixed point* for T-periodic orbits.

2.4 ZAD strategy

As it has been explained in the introduction, in order to make the output of the system v_o to follow a certain desired signal $w_{\text{ref}} > 0$, one can use the so called ZAD strategy. Setting $v_{\text{ref}} = w_{\text{ref}}/E$, and using the dimensionless variables, as in [8], [10] and [9], one first defines

$$s(t) := (x_1(t) - v_{\text{ref}}) + k_s\left(\dot{x}_1 - \dot{v}_{ref}\right), \tag{2.10}$$

where parameter k_s is a time constant associated with first order dynamics of the error surface $s(t) = 0$. Taking into account that our choice here is to consider v_{ref} as a constant, equation (2.10) can be simplified as

$$s(t) := (x_1(t) - v_{\text{ref}}) + k_s \dot{x}_1. \tag{2.11}$$

Once $s(t)$ is defined, ZAD strategy consists on finding the appropriate value of d_k by imposing function $s(t)$ to have zero average at each iteration, that is

$$\int_{kT}^{(k+1)T} s(t)dt = 0, \ \forall k \in \mathbb{Z}. \tag{2.12}$$

In order to solve equation (2.12), one can obtain an analytical expression in terms of the system's flow leading into a trascendental equation in d, or use an approximation of $s(t)$. This two options will be discussed on the next two sections.

2.4.1 ZAD strategy using the flow of the differential equations

As has been done in [1], one can write equation (2.12) in terms of the flow of the differential equations. Eliminating $\dot{x}_1$ in equation (2.11) using equations (2.3), it is easy to see that equation (2.12) can be written as

$$0 = \int_{kT}^{(k+1)T} s(t)dt = (1 - \gamma k_s, k_s) \int_0^T \Phi(t, x_0, d_k)dt - v_{\text{ref}}T, \tag{2.13}$$

where x_0 and d_k are the current value of the system state variables and duty cycle at time kT respectively. The expression of the integral of the flow is given by

$$\begin{aligned} \int_0^T \Phi(t, x_0, d_k)dt &= TA^{-1}B_1 d + A^{-1}\left[(e^{AT} - I)(x_0 + A^{-1}B_1) + \right. \\ &\quad \left. (e^{ATd_k/2} - e^{AT(1-d_k/2)})A^{-1}B_1\right]. \end{aligned} \tag{2.14}$$

Finally, equation (2.13) together with equation (2.14) gives an implicite expression which can be solved numerically with respect to d_k at each sampling period although it increases considerably computation costs.

2.4.2 Affine approximation of $s(t)$

In order to avoid solving equations (2.13) and (2.14) and reduce the complexity of the hardware implementation, one can consider an affine approximation of $s(t)$, as suggested in [3] and [4]. With that assumption, $s(t)$ can be approximated in $(kT, (k+1)T)$ as

$$s(t) = \begin{cases} s(kT) + t\dot{s}_1(kT), & t \in S_1 \\ s(kT) + d_kT/2\dot{s}_1(kT) + (t - d_kT/2)\dot{s}_2(kT), & t \in S_2 \\ s(kT) + d_kT/2\dot{s}_1(kT) + \\ (T - d_kT)\dot{s}_2(kT) + (t - T + d_kT/2)\dot{s}_1(kT), & t \in S_3 \end{cases},$$

where

$$\begin{aligned} S_1 &= [kT, kT + d_kT], \\ S_2 &= (kT + d_kT/2, (k+1)T - d_kT/2), \\ S_3 &= [(k+1)T + d_kT/2, (k+1)T) \end{aligned}$$

and $\dot{s}_1(kT)$ and $\dot{s}_2(kT)$ are two different slopes given by $\dot{s}(t)$ in $t = kT$ with $u = B_1$ and $u = B_2$ respectively. That is, differentiating expression (2.11) with respect to time, one obtains

$$\dot{s}(t) = -\gamma x_1 + x_2 + k_s(-\gamma\dot{x}_1 + \dot{x}_2).$$

Now, using the system equations (2.3) to eliminate the derivatives $\dot{x}_i$, $\dot{s}_i$ we obtain

$$\dot{s}_1(kT) = -\gamma x_1 + x_2 + k_s(-\gamma(-\gamma x_1 + x_2) - x_1 + 1)$$

for $u = B_1$, and

$$\dot{s}_2(kT) = -\gamma x_1 + x_2 + k_s(-\gamma(-\gamma x_1 + x_2) - x_1)$$

for $u = B_2$.
Finally, using this piecewise affine approximation of $s(t)$ in equation (2.12), one can isolate d_k and obtain

$$d_k = \frac{2s(kT) + T\dot{s}_2(kT)}{T(\dot{s}_2(kT) - \dot{s}_1(kT))} \tag{2.15}$$

with $0 \leq d_k \leq 1$.

2.5 Jacobian of the one and two iterated Poincaré map

In order to obtain stability properties or bifurcation conditions we will need the Jacobian of the one and two iterated Poincaré map, $DP(x_0, d)$ and $DP^2(x_0, d_1, d_2)$, where $P^2(x_0, d_1, d_2) = P(P(x_0, d_1), d_2)$.
As d depends on x_0 through the ZAD condition, the Implicit Function Theorem has to be applied in order to obtain $\partial d/\partial x_0$. Let us represent the ZAD equation (2.13) as $f_1(x_0, d) = 0$. It is not difficult to see that the conditions needed to apply this Theorem to this equation are fulfilled and, therefore, $DP(x_0, d)$ can be computed as

$$DP(x_0, d) = \frac{\partial P}{\partial x_0} - \frac{\partial P}{\partial d} \underbrace{\frac{\partial f_1/\partial x_0}{\partial f_1/\partial d}}_{-\partial d/\partial x_0}. \tag{2.16}$$

In order to obtain $DP^2(x_0, d_1, d_2)$, let us define

$$f_2(x_0, d_1, d_2) := f_1(x_1, d_2) = 0,$$

where $x_1 = P(x_0, d_1)$, as the ZAD equation (2.13) at the second iteration. Taking into account that d_1 depends on x_0 via the ZAD condition at the first iteration, $f_1 = 0$, we can calculate $\partial d_2/\partial x_0$, using again the Implicit Function Theorem, as

$$\frac{\partial d_2}{\partial x_0} = -\frac{\frac{\partial f_2}{\partial x_0} + \frac{\partial f_2}{\partial d_1}\frac{\partial d_1}{\partial x_0}}{\frac{\partial f_2}{\partial d_2}}, \tag{2.17}$$

where $\partial d_1/\partial x_0$ is obtained via the aplication of the same Theorem in equation $f_1 = 0$. With all these results, $DP^2(x_0, d_1, d_2)$ is given by

$$DP^2(x_0, d_1, d_2) = \frac{\partial P^2}{\partial x_0} - \frac{\partial P^2}{\partial d_1} \underbrace{\frac{\partial f_1/\partial x_0}{\partial f_1/\partial d_1}}_{-\partial d_1/\partial x_0} + \frac{\partial P^2}{\partial d_2}\frac{\partial d_2}{\partial x_0}, \tag{2.18}$$

where $\partial d_2/\partial x_0$ is obtained in equation (2.17).

Chapter 3

Two parameter bifurcation analysis: previous results

3.1 Introduction

In order to go forward from previous works, we will expose firstly in this chapter a brief overview to the state of the art on bifurcation analysis in a buck converter controlled by the ZAD strategy.
On this context, two different research lines have been parallely developed, an analytical (Fossas *et al.* [1]) and a numerical one (Angulo *et al.* [3]). In this last one, also the linear (in fact affine) approximation of the error surface $s(t)$ is used (see section 2.4.2).

3.2 Previous analytical results

As one of our main goals is to go forward the analytical results presented in [1], we present in this section a brief review to the most important results given in that reference, distinguishing between analytical conditions for periodic orbits and bifurcation analysis.

3.2.1 Periodic orbits

The strongest foundation of almost all analytical results concerning to period orbits is the next Lemma which proof is given in [1].

Lemma 3.1. *Given a linear system*

$$\dot{x} = Ax + u \tag{3.1}$$

where A is hyperbolic, u is piecewise linear and L-periodic, such that $\int_0^L u(t) = 0$, then there exists a unique L-periodic solution $x = x_p(t)$ such that $\int_0^L x_p(t)dt = 0$.

In order to show that system (2.4) verifies the conditions of the Lemma, let us apply the change of variables

$$\begin{aligned} e(t) &= x_1(t) - v_{\text{ref}} \\ s(t) &= e(t) + k_s\dot{e}(t) \end{aligned}$$

leading matrix A and function u into $\tilde{A}$ and $\tilde{u}$ such that $\int_0^T \tilde{u}dt = 0$ if, and only if,

$$d = v_{\text{ref}}. \tag{3.2}$$

Therefore, if $d_k = v_{\text{ref}}\ \forall k$, there exists a unique T-periodic solution, $(e_p(t), s_p(t))$, which satisfies

$$\int_0^T \begin{pmatrix} e_p(t) \\ s_p(t) \end{pmatrix} dt = 0,$$

which is exactly the ZAD condition.
On the other hand, solving equation

$$P(x_0, d) = x_0, \tag{3.3}$$

where $P(x_0, d)$ is defined in equation (2.9), one can also find the initial condition for a T-periodic orbit, which is given by

$$x_0^* = -A^{-1}B_1 + (I - e^{AT})^{-1}(e^{A\frac{Td}{2}} - e^{AT(1-\frac{d}{2})})A^{-1}B_1. \tag{3.4}$$

Summarizing, for each $d_k = d$ (constant), there exists a unique T-periodic solution of system (2.4) with intial conditions given by (3.4). In addition, this unique solution satisfies ZAD condition if $d = v_{\text{ref}}$.

Concerning to $2T$-periodic orbits, only saturated ones have been analytically investigated in [1], that is, $2T$-periodic solutions with duty cycles $(1, d_2)$ and $(d_1, 0)$. Solving equation

$$P\left(P\left(x_0, 1\right), d_2\right) = x_0, \tag{3.5}$$

the initial conditions for a $(1, d_2)$ $2T$-periodic orbit, $x^{**}_{0,1d_2}$, are found.

3.2.2 Period doubling and corner collision bifurcation curves

Two kind of bifurcations are analyzed in [1], a usual period doubling and a corner collision.
The first bifurcation is found using the fact that a necessary condition for such a phenomena to occur is that one of the eigenvalues of the Jacobian of the Poincaré map evaluated at the fixed point equals minus one. So, the expression

$$\det(DP(x_0^*, d) + I) = 0, \tag{3.6}$$

where x_0^* is given by (3.4) and $d = v_{\text{ref}}$ in order to verify the ZAD condition, represents the period doubling bifurcation curve.
This bifurcation curve is mentioned in [1] to be a subcritical period doubling. In fact, as we will later show, it is a subcritical or supercritical flip depending on the value of v_{ref}. One of our main goals is to explain how this change on the systems behaviour is given so we will later return to that topic.

With regard to the corner collision bifurcation, let us first use the three dimensional autonomus version of the system, that is, we add time as a new state variable. Then, we consider as switching surfaces the set of state variables in this three dimensional space across which the system topology changes from $u = B_1$ to $u = B_2$ or vice versa. It can be shown that an orbit collides the intersection of those surfaces when $d = 1$ or $d = 0$ and, therefore, when an orbit gets saturated a corner collision bifurcation takes place (see [5] for more details). In other words, the corner collision occurs when one of the two duty cycles of the 2-periodic solutions reaches $d = 1$ or $d = 0$. On the other hand, Lemma 3.1 applied to a $2T$-periodic orbit implies $d_1 + d_2 = 2v_{\text{ref}}$ in order to ZAD be fullfilled in the whole $2T$ period. Notice that the saturation will be produced to a $(1, d_2)$ orbit only for $v_{\text{ref}} \in (\frac{1}{2}, 1]$, and to $(d_1, 0)$ saturated orbit for $v_{\text{ref}} \in [0, \frac{1}{2})$. For $v_{\text{ref}} = \frac{1}{2}$, the saturation will given by both values simultaneously, i. e., to $(1, 0)$ $2T$-periodic orbits.
With all previous explanations in mind, the corner collision curve is defined for $v_{\text{ref}} \geq \frac{1}{2}$ by equation (2.13) using $x^{**}_{0,1d_2}$ as initial condition and $d_2 = 2v_{\text{ref}} - 1$, and for $v_{\text{ref}} \leq \frac{1}{2}$ using $x^{**}_{0,d_1 0}$ as initial condition and $d_1 = 2v_{\text{ref}}$. This intial condition would be found analogously as $x^{**}_{0,1d_2}$ was.

In Figure 3.1 we finally present both curves. There exist there five labeled points.
Point D corresponds to $v_{\text{ref}} = 0.5$ and separates the saturation of the 2-periodic branches to 1 from the saturation to 0. At that point the corner

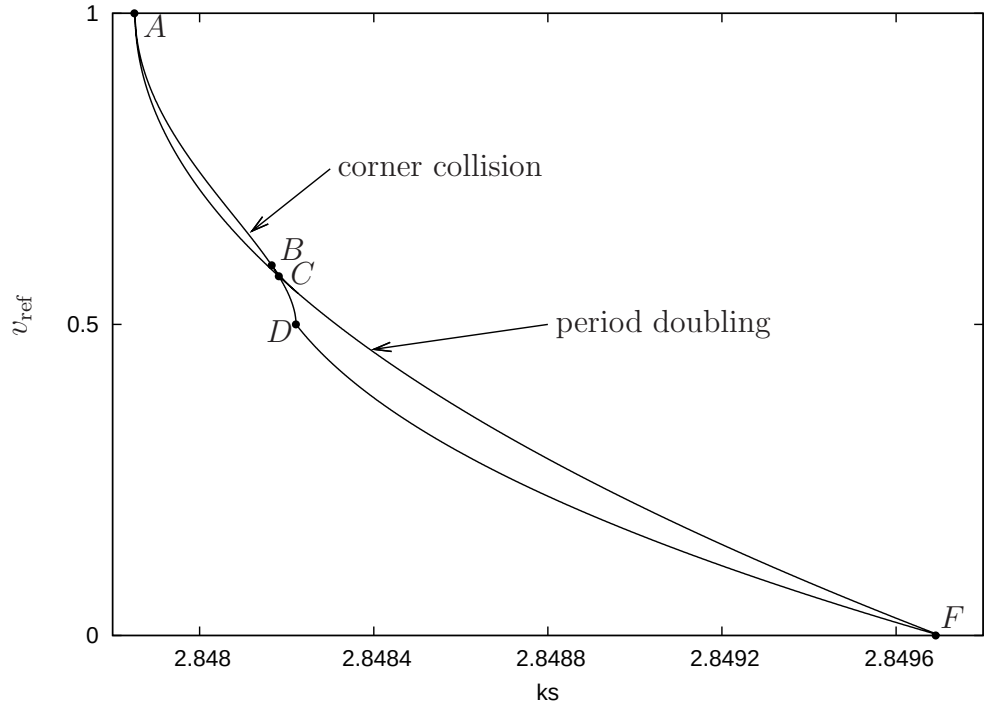

Figure 3.1: Period doubling and corner collision curves found in [1].

collision bifurcation curve is not smooth.
Points A and F are meeting points of both curves respectively corresponding to maximun and minimum values of the dimensionless reference signal v_{ref}. As it is shown in [1], both curves collide tangently and vertically in A but not in F.
Point C represents also an intersection point between both curves where both bifurcations occur at the same time.
As points A, F and C are intersection points between the period doubling and the corner collision curves, they are codimension two points. However, as it is mentioned in [1], there exists also another codimension two point labeled as B and given by the meeting of the corner collision and a saddle node bifurcation curve that emgerges from B. Although this curve is not shown in Figure 3.1, it plays an important role on the explanation of the whole behaviour of the system in parameter space and, therefore, we will later calculate it.

On the other hand, in order to explain the behaviour of the system in several regions of the parameter space, some one dimensional parameter bifurcation diagrams are also shown in [1]. As we will later go further on these

diagramns we do not show them here.

3.3 Using the affine approximation of $s(t)$

We give in this section a brief review on the results presented by Angulo *et al.* ([3]). As mentioned before, it is used in that work not only numerical methods but also an affine approximation of the error surface $s(t)$, already explained in section 2.4.2. Unfortunately, there exist some differences between the results presented in the cited work and the analytically found ones presented in previous section. We will show in this section these differences and we will justify them in next chapters.

In contrast to [1], a whole analysis in k_s range parameter is done in [3] for a fixed v_{ref}. As it is shown there, several period doubling and corner collision bifurcations appear, decreasing k_s, on the transition from the fixed point to chaos. More specifically, a first and a second period doubling and corner collsion bifurcations are analyzed and such bifurcation curves are ploted in the two dimensional parameter space. Also, a full discussion about the behaviour of non-saturated and saturated $2T$ and $4T$-periodic orbits is presented. However, no crossing point C is detected between both bifurcation curves. On the contrary, corner collision curves remain on the left hand side of period doubling ones, so this last bifurcation is for every v_{ref} a supercritical flip bifurcation.
This last fact causes the main difference between the use of the affine approximation of $s(t)$ (in fact just the use of numerical methods) with the analytical results.

Chapter 4

Two parameter bifurcation analysis: further results

4.1 Introduction

The existence of the crossing point between the period doubling and the corner collision bifurcation curves, labeled as C in Figure 3.1, implies two clearly different shapes of the 2-periodic orbits branches in one dimensional bifurcation diagrams. For v_{ref} "sufficiently above" the point C, a usual subcritical flip bifurcation takes place, and for v_{ref} "sufficiently below" this bifurcation is supercritical[1]. In other words, both situations are shown in Figure 4.1.

As one of our main goals is to explain how this change on the period doubling

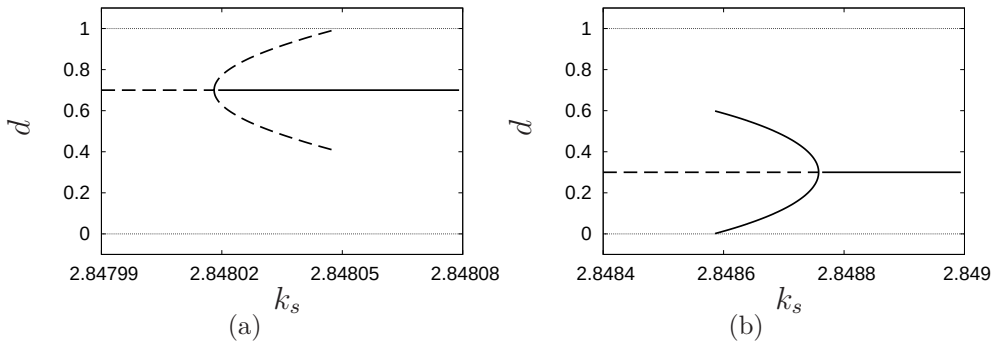

Figure 4.1: One parameter bifurcation diagrams for $v_{\text{ref}} = 0.7$ (a) and $v_{\text{ref}} = 0.3$ (b). Unstable and stable orbits are represented by dashed and solid lines respectively.

[1]We will further explain what exactly "sufficiently below and above" mean.

bifurcation behaviour takes place, we will later give, together with the eigenvalues evolution, several one dimensional bifurcation diagrams where we will explain how these curves have been analytically calculated. As, essentially, the answer remains in the already commented saddle node bifurcation, we will also add this bifurcation curve to the 2 dimensional bifurcation diagram discussed in section 3.2.2.
On the other hand, using the concepts of virtual and feasible solutions, we will also complete all possible one dimensional bifurcation diagrams with saturated periodic orbits together with a detailed explanation of the regions of existence in parameter space of all possible one and two periodic objects.
Eventually, we will show that numerical simulations do not fulfill completely what was expected from the analytical results. In next chapter we will give a possible explanation to this fact, together with the differences presented also using the affine approximation of $s(t)$, introducing a perturbation of the ZAD condition.

4.2 Feasible and virtual periodic orbits

Before going into detail on one dimensional bifurcation diagrams, let us see how these are analytically obtained.

4.2.1 Analytical procedure

In order to find the initial condition for a 2-periodic orbit with non-saturated duty cycles of the form (d_1, d_2), let us first fix v_{ref}. Defining

$$P^2(x_0, d_1, d_2) = P(P(x_0, d_1), d_2),$$

this initial condition must satisfy the equation

$$P^2(x_0, d_1, d_2) = x_0,$$

which solution is

$$\begin{aligned} x^{**}_{0,d_1 d_2} = \quad & \Big(-e^{2\,AT} + e^{AT\left(2-\frac{d_1}{2}\right)} - e^{AT\left(1+\frac{d_1}{2}\right)} \\ & + e^{AT\left(1-\frac{d_2}{2}\right)} - e^{AT\frac{d_2}{2}} + 1\Big)\left(e^{2\,AT} - I\right) A^{-1}B, \end{aligned} \tag{4.1}$$

where the notation used here is to denote by

$$x^{\overbrace{*\cdots*}^{n \text{ times}}}_{i,d_1 \ldots d_n}$$

the $i-$th iterated by the Poincaré map of an n-periodic orbit with duty cycles $(d_1, \ldots, d_n)$.
Notice that setting $d_1 = 1$, the initial condition for a 2-periodic orbit with one saturated duty cycle, $x^{**}_{0,1d_2}$, would be obtained as has been mentioned in section 3.2.1.
In order to force the ZAD condition be fulfilled at both iterations, let us first recall that

$$x^{**}_{1,d_1d_2} = P(x^{**}_{0,d_1d_2}, d_1).$$

Then, from equation (2.13), both duty cycles must verify equations

$$(1 - \gamma k_s, k_s) \int_0^T \Phi(t, x^{**}_{0,d_1d_2}, d_1)dt - v_{ref}T = 0 \tag{4.2}$$

$$(1 - \gamma k_s, k_s) \int_T^{2T} \Phi(t, x^{**}_{1,d_1d_2}, d_2)dt - v_{ref}T = 0. \tag{4.3}$$

However, as it has been discussed in section 3.2.2, applying Lemma 3.1 to a $2T$-periodic orbit, ZAD strategy is fulfilled in the whole $2T$ period if both duty cycles verify

$$d_1 + d_2 = 2v_{\text{ref}}. \tag{4.4}$$

Therefore, just one of equations (4.2) or (4.3) must be solved in order to find one of the duty cycles satisfying ZAD condition. The ohter duty cycle can be found using equation (4.4).

Finally, we will proceed as follows. Let us first fix d_1. Using equation (4.4) we find d_2 and, at last, from equation (4.2) or (4.3) we obtain k_s. Now, repeating this procedure for every $d_1 \in [v_{\text{ref}}, 1]$ or $d_1 \in [0, v_{\text{ref}}]$ (depending on whether $v_{\text{ref}} \geq 0.5$ or not), the 2-periodic solutions verifying ZAD strategy at each period in one dimensional parameter space will be obtained for every v_{ref}.

4.2.2 One dimensional bifurcation diagrams

Before going forward on the explanation of the transition between the situations shown in Figures 4.1(a) and 4.1(b), let us first justify the stability properties already shown in that figures.
Evaluating the Jacobian of the Poincaré map $DP(x_0)$, already obtained in section 2.5, at the fixed point x_0^* given by equation (3.4), and proceeding as in section 4.2.1, we obtain the eigenvalues of $DP(x_0^*)$ shown in Figure 4.2. Notice that there exists a value of k_s where one eigenvalue reaches -1 for which the period doubling takes place, and, in both figures, the fixed point

remains stable at the right hand side while unstable on the left one. Although these eigenvalues are only shown for two values of v_{ref}, this situation remains the same for all of them.

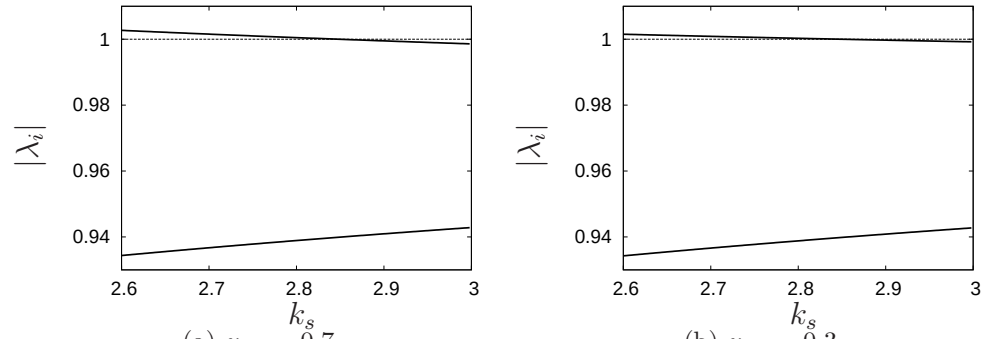

(a) $v_{\text{ref}} = 0.7$ (b) $v_{\text{ref}} = 0.3$

Figure 4.2: Eigenvalues modulus of $DP(x_0^*)$

Proceeding in a similar manner, we evaluate the Jacobian of the second iterated Poincaré map, $DP^2(x_0)$ already explained in section 2.5, at $x^{**}_{0,d_1 d_2}$ given by equation (4.1). The evolution of the critical eigenvalue is shown in Figure 4.3 for two values of v_{ref} while the other one remains with modulus lower than 1. We will see below how the system evolves from the situation shown if Figure 4.3(a) to the one shown in Figure 4.3(b).

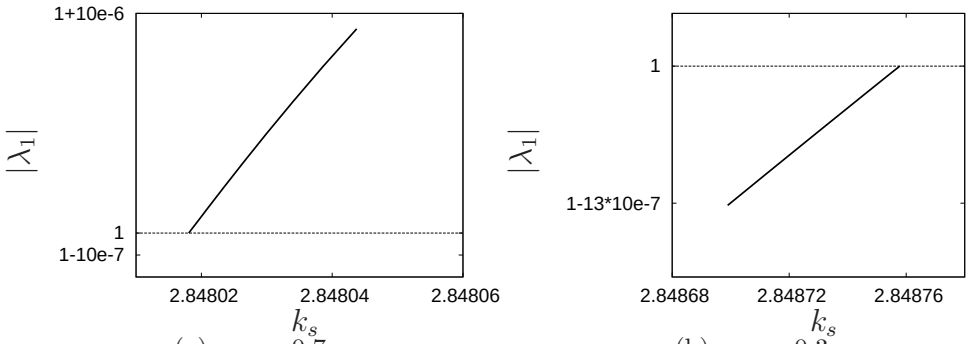

(a) $v_{\text{ref}} = 0.7$ (b) $v_{\text{ref}} = 0.3$

Figure 4.3: Critical eigenvalue modulus of $DP^2(x_0^{**})$

Notice that, as shown if Figure 4.3, the 2-periodic orbit is unstable for $v_{\text{ref}} = 0.7$ and stable for $v_{\text{ref}} = 0.3$ so, together with the results from Figure 4.2, we finally demonstrate that period doubling bifurcation is subcritical or

supercritical depending on the value of v_{ref}.

In order to explain the transition between these to behaviours, we have first to take into account what are the basic differences between these two situations.
First of all, a change on the stability and in the orientation of the 2-periodic orbits takes place. As we will see and as it has briefly mentioned in section 3.2.2, these changes are due to the "appearance"[2] of a saddle node bifurcation at the point labeled in Figure 3.1 as $B = (\tilde{k}_s, \tilde{v}_{\text{ref}})$.
On the other hand, it should also be remarked that on the first case the corner collision takes place on the right hand side of the period doubling and, on the contrary, it is on the left hand side in the second case. These two facts are separated by the existence of the intersection point between the corner collision and the period doubling bifurcations curves, as has been mentioned in section 3.2.2. This point is labeled as $C = (\breve{k}_s, \breve{v}_{\text{ref}})$ in Figure 3.1.
Finally, we should also notice that, in the first case, the saturation is produced by one duty cycle equal to 1, and in the second one, it equals 0. As has been remarked in section 3.2.2, these last behaviours are separated by the straight line $v_{\text{ref}} = 0.5$.

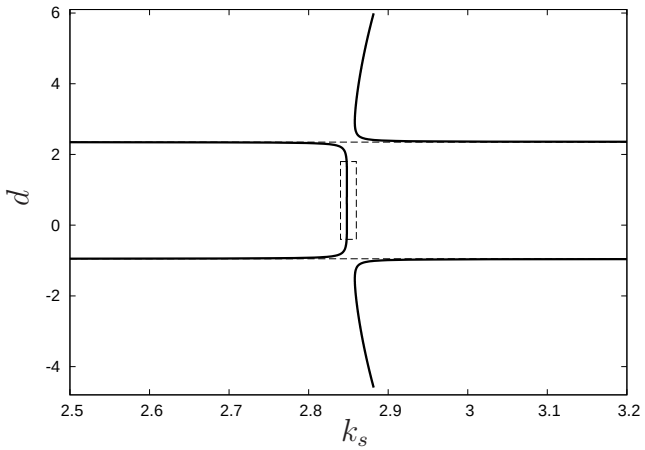

Figure 4.4: Complete nonsaturated bifurcation diagram for $v_{\text{ref}} = 0.7$, $0.7 \leq d_2 \leq 6$ and d_2 given by equation (4.4).

Once the main differences between situations of figures 4.1(a) and 4.1(b) have been presented and in order to explain in an accurate manner all the facts involved in this transition, let us neglet the saturation condition and

[2]We will later clarify the meaning of this term here.

obtain a whole picture of the one dimensional bifurcation diagram for $v_{\text{ref}} > \tilde{v}_{\text{ref}}$ (before the saddle node bifurcation "appears"), which is shown in Figure 4.4. There one can see that the bifurcation diagram has two horizontal assymptotes for further values of d. As we shall see, these two objects do not reach values of d between 0 and 1 for other values of v_{ref} at the same time, and, therefore, all the analysis on the dynamics can be carried out just considering the local box of Figure 4.4 shown in Figure 4.5.

There one can see that the branches of the period doubling are not given by a parabola but (locally) by a fourth degree polynomial of the form

$$-k_s(d) = a_1(d - v_{\text{ref}})^4 + a_2(d - v_{\text{ref}})^2 + a_3, \tag{4.5}$$

which is symmetric respect to $d = v_{\text{ref}}$. We also show in Figure 4.6 the evolution of the critical eigenvalue of $DP^2(x^{**}_{0,d_1d_2})$. Notice that this eigenvalue reaches $+1$ at the period doubling bifurcation but also at a saddle node one (points M and m_1 or m_2 respectively).
The saturation condition implies the existence of two different regions for the duty cycle d, a feasible, $[0, 1] \subset \mathbb{R}$, and a virtual one, $\mathbb{R}\backslash[0, 1]$. As the symmetric branches of the polynomial represent for every k_s different 2-periodic orbits of the form (d_1, d_2), this differentiation leads us to state these next two complementary definitions.

Definition 4.1. *A (d_1, d_2) 2-periodic orbit is said to be* **feasible** *if $0 \leq d_i \leq 1$ for $i = 1, 2$. It is said to be* **virtual** *or* **not feasible** *otherwise.*

In the situation shown in Figure 4.5, notice that there exists a pair of 2-peridoic orbits emerging at the saddle node bifurcation but they remain virtual as long as at least one of the points m_1 or m_2 marked in Figure 4.5 is located outside the feasible domain. However, not only the position of these points but the shape of the fourth degree polynomial changes as v_{ref} does making these points to become feasible (or "appear") leading the system to different dynamical behaviours. The main changes that take place as v_{ref} varies are the position of the local minima m_1 and m_2 (the saddle node bifurcation), and the local maximum M (the period doubling bifurcation). Concerning to the position of this last point, notice that its vertical position changes with the one of the symmetry axis since this line is located at $d = v_{\text{ref}}$.
In Figure 4.7 we show again the period doubling and the corner collision bifurcation curves together with the feasible saddle node one. Several cross sections are also labeled and shown in Figure 4.8, which correspond to several characteristic situations on the shape of the 2-periodic branches represented

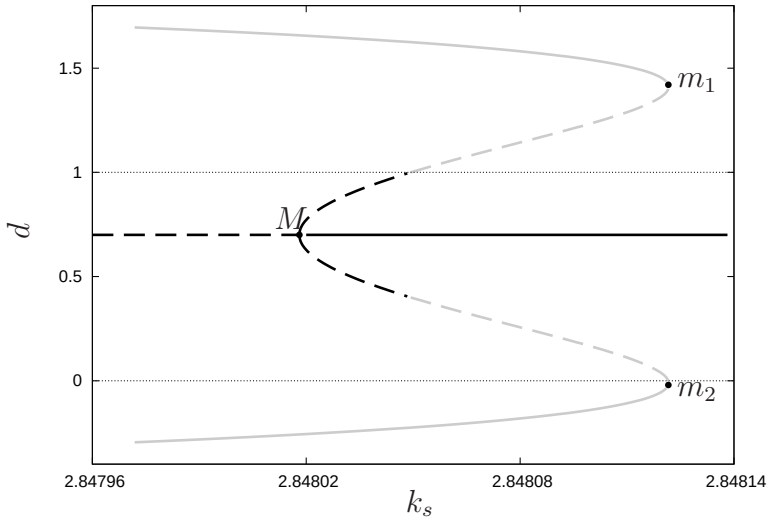

Figure 4.5: Complete nonsaturated bifurcation diagram for $v_{\text{ref}} = 0.7$, $0.7 \leq d_1 \leq 1.7$ and d_2 given by equation (4.4) (blow up from Figure 4.4). Solid and dashed lines represent stability and instability respectively, black and gray lines represent feasible and virtual 2-periodic orbits respectively.

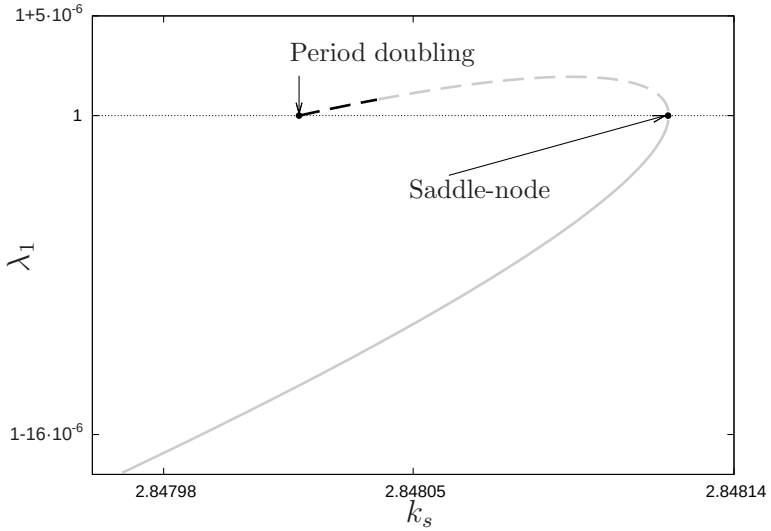

Figure 4.6: Critical eigenvalue of $DP^2(x^{**}_{0,d_1 d_2})$. Black and gray correspond respectively to feasible and virtual solutions. Solid and dashed imply, respectively, stability and instability.

by the fourth degree polynomial.
First of all, the position of point M leads us the discuss two different behaviours separated by point D in Figure 4.7.

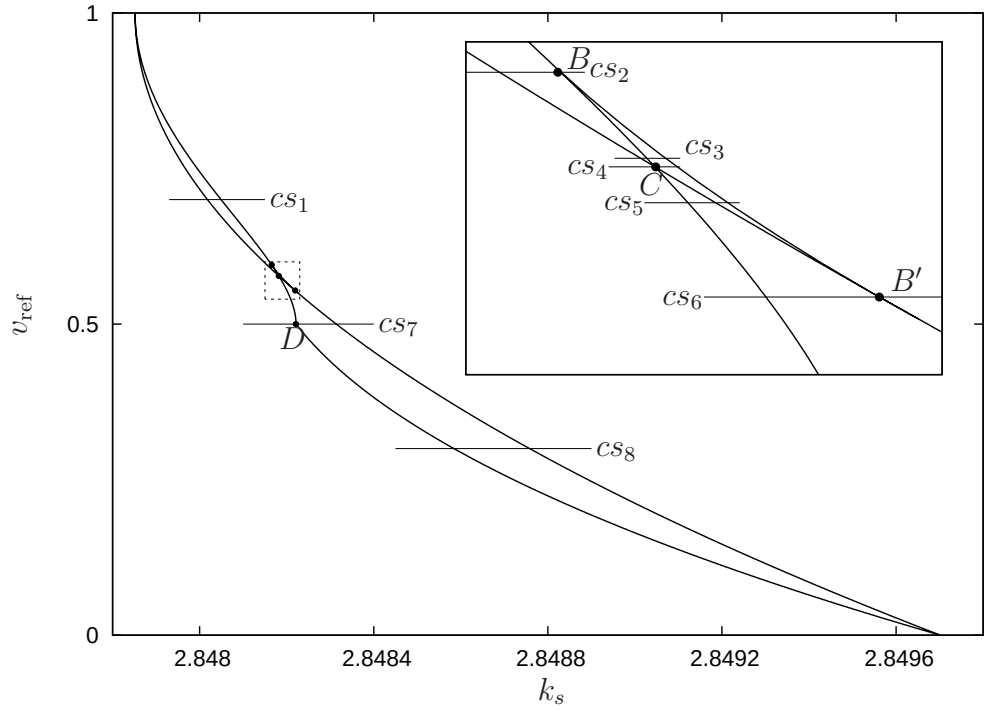

Figure 4.7: Period doubling, corner collision and feasible saddle-node bifurcation curves. The one-dimensional bifurcation diagrams across the lines marked with cs_i are shown in Figure 4.8.

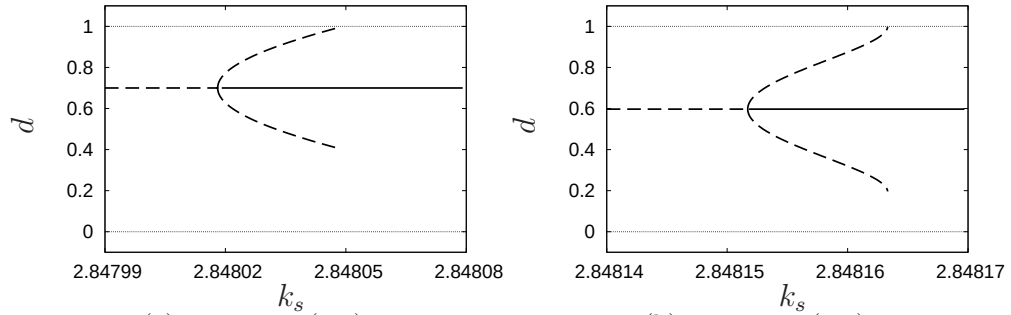

(a) $v_{\text{ref}} > \tilde{v}_{\text{ref}}$ (cs_1) (b) $v_{\text{ref}} = \tilde{v}_{\text{ref}}$ (cs_2)

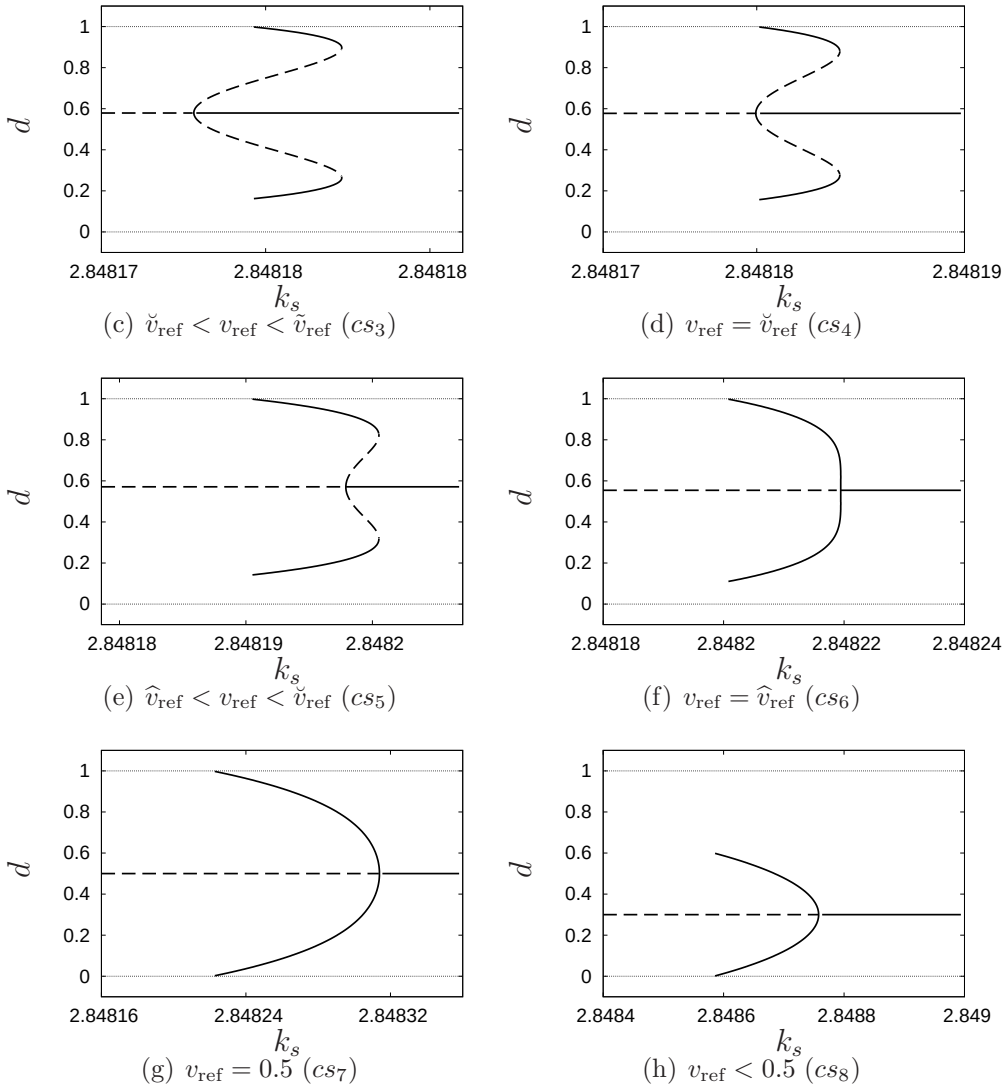

(c) $\breve{v}_{\text{ref}} < v_{\text{ref}} < \tilde{v}_{\text{ref}}$ (cs_3) (d) $v_{\text{ref}} = \breve{v}_{\text{ref}}$ (cs_4)

(e) $\widehat{v}_{\text{ref}} < v_{\text{ref}} < \breve{v}_{\text{ref}}$ (cs_5) (f) $v_{\text{ref}} = \widehat{v}_{\text{ref}}$ (cs_6)

(g) $v_{\text{ref}} = 0.5$ (cs_7) (h) $v_{\text{ref}} < 0.5$ (cs_8)

Figure 4.8: One dimensional bifurcation diagrams. Each plot corresponds to a cross section labeled as cs_i in Figure 4.7.

Point D

Due to the symmetry of the fourth degree polynomial with respect to the straight line $d = v_{\text{ref}}$, there exist two different behaviours depending on whether $v_{\text{ref}} > 0.5$ or not. In the first case, 2-periodic orbits become virtual due to the collision of the upper branch with the upper boundary of the feasible region $d = 1$, and the saturation is produced to 1. By contrast, if $v_{\text{ref}} < 0.5$, the lower branch collides first with the lower boundary of the

feasible region and the saturation of one of the duty cycles is produced to 0. Obviously, there exists a point, $D = (\check{k}_s, 0.5)$, which separates this two different behaviours and where the two branches collide both boundaries of the feasible region at the same value of k_s, and the saturation of the duty cylces are produced both to 1 and to 0. The corresponding one dimensional bifurcation diagram for $v_{\text{ref}} = 0.5$ is shown in Figure 4.8(g), which corresponds to the cross section cs_7 in Figure 4.7.

On the other hand, there exists a value of v_{ref} for which the saddle node bifurcation points, m_1 and m_2, become feasible. This leads us to discuss points B and B' of Figure 4.7.

Points B, B' and saddle node bifurcation curve

In the situation shown in Figure 4.5, coefficients a_1 and a_2 of equation (4.5) are positive and negative respectively. As v_{ref} decreases, a_2 increases so yielding points m_1, M and m_2 become closer. As the period doubling bifurcation point M always remains in the feasible region, that implies that there exists a value of v_{ref} for which the saddle node bifurcation points m_1 and m_2 become feasible. Therefore, there exists a codimension two point labeled as point $B = (\tilde{k}_s, \tilde{v}_{\text{ref}})$ where both the saddle node and the corner collision bifurcation occur for the same value of k_s. The corresponding one dimensional bifurcation diagram is shown in Figure 4.8(b), which corresponds to the cross section cs_2 of Figure 4.7.
From that moment, the saddle node bifurcation curve becomes feasible and it emerges from point B until it collides with the period doubling bifurcation curve at point $B' = (\widehat{k}_s, \widehat{v}_{\text{ref}})$ labeled in Figure 4.7. At that point, coefficient a_2 reaches zero and points m_1, M and m_2 of Figure 4.5 meet together and so do they for forward values of v_{ref} as a_2 becomes positive[3]. That is, the saddle node and the period doubling bifurcation curves become the same for $v_{\text{ref}} \leq \widehat{v}_{\text{ref}}$. Therefore, point B' is also another codimension two bifurcation point where the saddle node and the period doubling bifurcation occur at the same value of k_s. In other words, the unstable 2-periodic orbit is destroyed if $v_{\text{ref}} \leq \widehat{v}_{\text{ref}}$. The one dimensional bifurcation diagram for this case is shown in Figure 4.8(f), corresponding to the cross section cs_6 on Figure 4.7.
Due to the feasibility of the saddle node bifurcation points, there exists a region of coexistence of both feasible stable and unstable 2-periodic orbits between points B and B'. This region is bounded by the saddle node bifurcation curve on the right, and by the period doubling or the corner collision

[3]Notice that, as a_1 always remains positive, the fourth degree polynomial (4.5) will lose their two minimums for $a_2 \geq 0$.

curves on the left, depending on if v_{ref} is above or below the labeled point C.

This last distinction of the left boundaries of the feasible coexistence region leads us to discuss the last point of interest, point C.

Point C

Once the saddle node bifurcation points are located in the feasible region, the period doubling bifurcation point M remains on the left of the saturation point. Therefore, the coexistence of both 2-periodic orbits is bounded on the left by the corner collision curve.
As v_{ref} decreases, point M tends to move to the right while, on the contrary, the collision of the stable branches of the fourth degree polynomial with the boundaries of the feasible region (corner collision) moves to the left. Before points m_1, M and m_2 meet together, there exists a value of v_{ref} for which the corner collision and the period doubling occur for the same value of k_s. This is the point labeled in Figure 4.7 as point $C = (\breve{k}_s, \breve{v}_{\text{ref}})$, and whose one dimensional bifurcation diagram is shown in Figure 4.8(d), corresponding to cross section cs_4 in Figure 4.7.
After that moment, the region of feasible coexistence between both 2-periodic orbits is bounded on the left by the period doubling curve.

4.3 Regions of existence in parameter space and saturated orbits

From all previous results, we present in Figure 4.9 the regions of existence in parameter space of stable and unstable fixed point and 2-periodic orbits. The saddle node bifurcation curve is plotted as a gray curve when this bifurcation is located in the virtual region. A dashed line is also plotted to distinguish between the saturation of the stable 2-periodic orbit to 1 from saturation to 0.
As all bifurcation curves represent existence boundaries of different objects, each labeled region represents a region of coexistence of different objects.

In Figure 4.10, we also complement the one dimensional bifurcation diagrams shown in Figure 4.8 with 2-periodic orbits with one saturated duty cycle (saturated orbits). In the following discussions one can find the arguments for the existence of these kind of orbits.

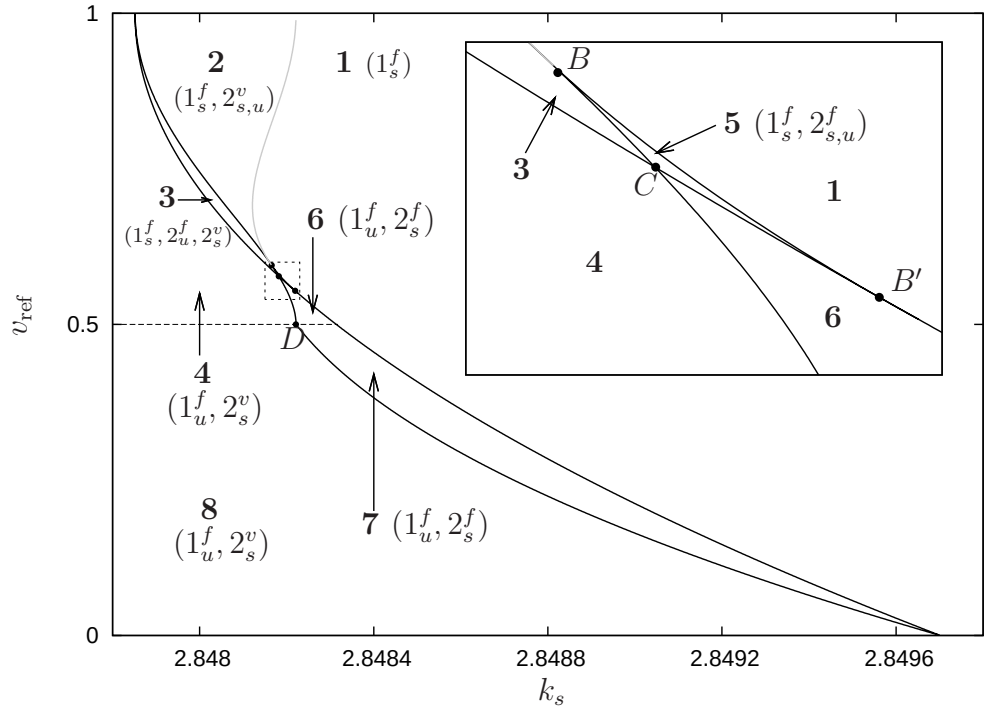

Figure 4.9: Regions of existence bounded by solid lines. Gray line represents virtual saddle-node bifurcation. Labeled zones are the next ones: **1**, stable fixed point; **2**, stable fixed point and virtual-stable and unstable 2-periodic orbits; **3**, stable fixed point, feasible-unstable 2-periodic orbits saturating to 1 and virtual-stable 2-periodic orbits; **4**, unstable fixed point and virtual-stable 2-periodic orbits (saturation to 1); **5**, stable fixed point, feasible-unstable 2-periodic orbits saturating to 1 and virtual-stable 2-periodic orbits; **6**, unstable fixed point and feasible-stable 2-periodic orbits saturating to 1; **7**, unstable fixed point and feasible-stable 2-periodic orbits saturating to 0; **8**, unstable fixed point and virtual-stable 2-periodic orbits (saturation to 0).

4.3.1 Stable fixed point

In this region, labeled with **1**, only the fixed point exists. For minor values of k_s, above B', this region is bounded by the saddle node bifurcation curve (both feasible and virtual), and by the period doubling bifurcation curve below this point. It is unbounded for greater values of k_s.
Due to this left-bounding of the saddle node bifurcation curve, no saturated orbits are possible in this region as there do not exist any 2-periodic solution, even feasible or virtual.

4.3.2 Stable fixed point and virtual-stable and unstable 2-periodic orbits

In this region, labeled with label **2**, there coexists the stable fixed point and the virtual stable and unstable 2-periodic orbits as k_s is located between the saddle node bifurcation and the corner collision while the period doubling bifurcation is produced on the left hand of this last one.
As the stable manifold of the virtual 2-periodic orbit remains on the virtual region, all feasible orbits are attracted to the fixed point. Therefore, saturated orbits are not possible in this region.

4.3.3 Stable fixed point, feasible-unstable and virtual-stable 2-periodic orbits

Labeled with **3**, this region is the one compressed by the period doubling, on the left, and the corner collision, on the right, bifurcation curves above point C. Therefore, there coexist an stable fixed point, a feasible-unstable 2-periodic orbit saturating to 1 and a virtual stable 2-periodic orbit.
As the stable manifold of the virtual-stable 2-periodic orbit intersects the feasible region, there coexist in this region an stable saturated to 1 2-periodic orbit and the stable fixed point.

4.3.4 Unstable fixed point and virtual-stable 2-periodic orbits

This region is bounded by the period doubling bifurcation curve above point C and by the corner collision one below. In this, the fixed point is unstable as k_s remains on the left hand of the period doubling bifurcation curve, and the 2-periodic stable orbit is virtual.
As the fixed point is unstable, the system will try to reach the stable but virtual 2-periodic orbit, so solutions with parameter values located in this region will remain in the feasible region boundaries, that is, the system will converge to 2-periodic orbits with one saturated duty cycle. Depending on if $v_{\text{ref}} > 0.5$ or not, the saturation will be produced, respectively, to 1 (region **4**) or to 0 (region **8**).

4.3.5 Stable fixed point and feasible-stable and unstable 2-periodic orbits

This region, labeled as **5**, is the one bounded on the right hand side by the saddle node bifurcation curve, and, on the left one, by the corner collision above point C and by the period doubling bifurcation curve below.
There coexist there the three different objects being all of them feasible. Therefore, solutions using values of k_s and v_{ref} located in that region could converge to the stable fixed point or to a stable 2-periodic with nonsaturated duty cycles. As parameters reach the nonsmooth corner collision boundary, one of the duty cycles tends to saturate to 1.
Due to the feasibility of the stable 2-periodic orbit no saturated orbits are possible in this region as there exists no attractor outside the boundaries of the feasible region.

4.3.6 Unstable fixed point and feasible-stable 2-periodic orbits

Below point C and between the period doubling and the corner collision bifurcation curves, the fixed point is unstable, the stable 2-periodic solutions are feasible and the unstable 2-periodic ones do not exist. Therefore, all orbits with parameters located in this region will converge to a non-saturated 2-periodic orbit as it is the unique attractor that exists there.
However, two different behaviours may be distinguished. As k_s gets closer to the corner collision bifurcation curve one duty cycle will tend to saturate to 1 (region **6**) or to 0 (region **7**) depending on if $v_{\text{ref}} > 0.5$ or not.

With all previous explanations we can finally add to the one dimensional bifurcation diagrams of Figure 4.8 saturated orbits of the form $(1, d_2)$ and $(d_1, 0)$, as Figure 4.10 shows. Notice that, as a summary, 2-periodic orbits with one saturated duty cycle only exist on the left hand side of the corner collision bifurcation.

4.4 Numerical simulations

In this section we expose the numerical results when simulating the system for two different situations, for $v_{\text{ref}} = 0.7$ (Figure 4.10(a)) and for $v_{\text{ref}} = 0.3$ (Figure 4.10(h)). We consider these values as typical examples for the two situations discussed in previous sections: a subcritical and a supercritical period doubling bifurcation respectively. However, before discussing these

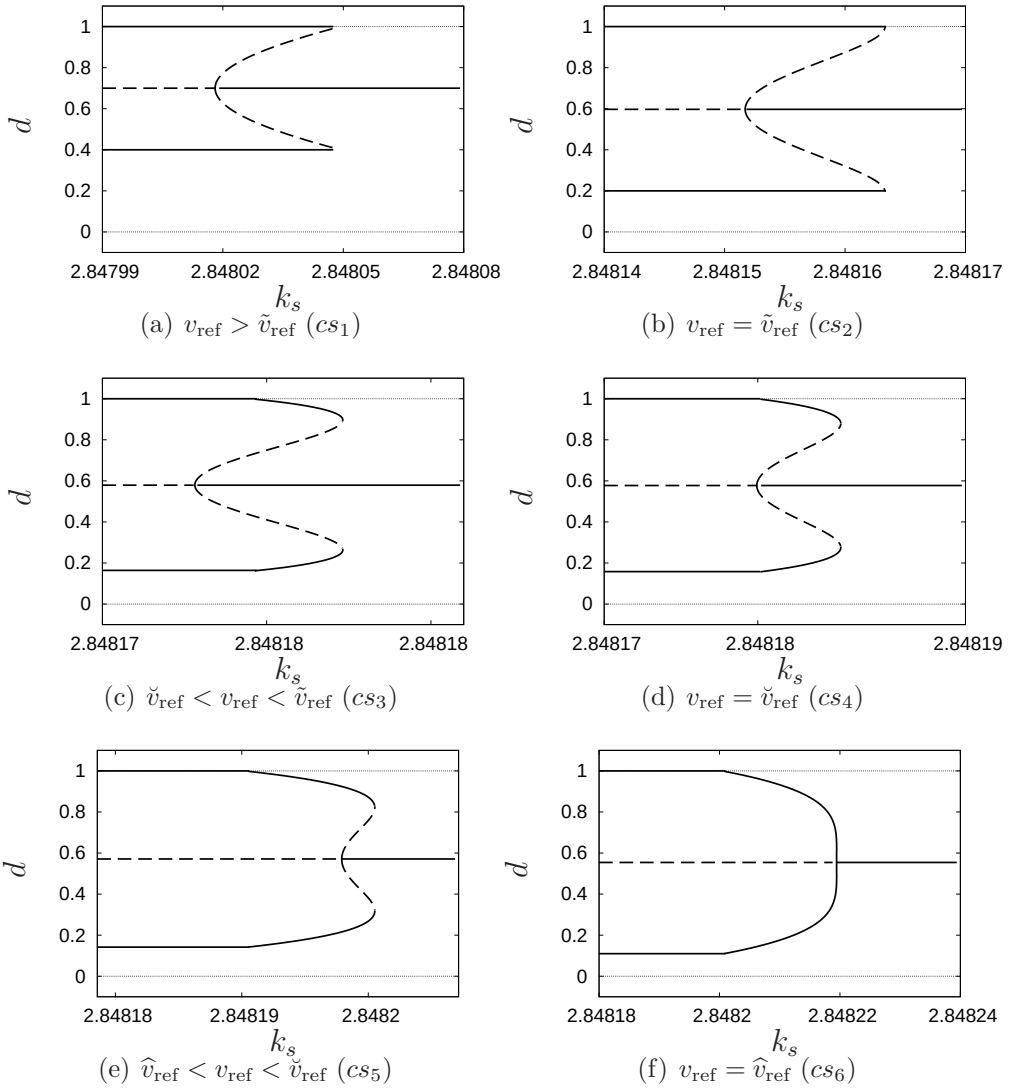

(a) $v_{\text{ref}} > \tilde{v}_{\text{ref}}$ (cs_1) (b) $v_{\text{ref}} = \tilde{v}_{\text{ref}}$ (cs_2)

(c) $\breve{v}_{\text{ref}} < v_{\text{ref}} < \tilde{v}_{\text{ref}}$ (cs_3) (d) $v_{\text{ref}} = \breve{v}_{\text{ref}}$ (cs_4)

(e) $\widehat{v}_{\text{ref}} < v_{\text{ref}} < \breve{v}_{\text{ref}}$ (cs_5) (f) $v_{\text{ref}} = \widehat{v}_{\text{ref}}$ (cs_6)

results, let us explain how these simulations have been obtained and what would one expect from them.

The numerical one dimensional bifurcation diagrams presented in this section have been obtained iterating the Poincaré map (2.9) using the same initial condition for several values of k_s and for these two values of v_{ref}. At each iteration, equation (2.13) has been solved using a simple Newton-Raphson method with a tolerance of 10^{-12} in order to find the value of d which makes ZAD be fulfilled at the current iteration.

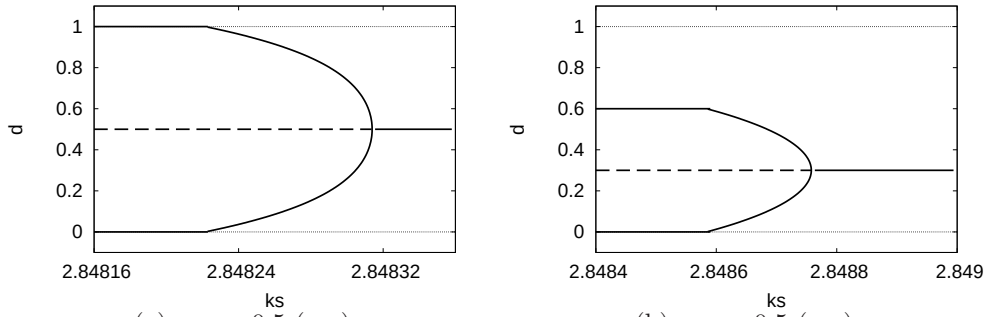

(g) $v_{\text{ref}} = 0.5$ (cs_7) (h) $v_{\text{ref}} < 0.5$ (cs_8)

Figure 4.10: One dimensional bifurcation diagrams. Each plot corresponds to a cross sections labeled as cs_i in Figure 4.7. This is the same Figure as 4.8 but saturated orbits have been added.

Concerning to what one expects from that simulations, let us distinguish between both situations.

4.4.1 Numerical simulations for the subcritical flip bifurcation, $v_{\text{ref}} = 0.7$

From what has been exposed in previous sections, it is clear that, when trying to simulate the system for v_{ref} such that the saddle node is not feasible (see Figure 4.10(a)), a 2-periodic orbit with one saturated duty cycle should be obtained for k_s located on the left hand side of the period doubling bifurcation. It is also clear that the fixed point should be obtained for k_s located on the right hand side of the corner collision bifurcation. However, for k_s between these two bifurcations both stable objects coexist (region **3** of Figure 4.9 and section 4.3.3), so the system behaviour in this region will depend on in which stable manifold the initial duty cycle is located. As d is not an state variable but it is related with them through the ZAD condition, let us consider the family of curves $\zeta(x_0)$ formed by points (k_s, d) shuch that, for a certain initial condition x_0, the ZAD condition is fulfilled at the first iteration,

$$\zeta(x_0) = \left\{ (k_s, d) \mid (1 - \gamma k_s, k_s) \cdot \int_0^T \Phi(t, x_0, d)dt - v_{\text{ref}}T = 0 \right\},$$

plotted in Figure 4.11(a) as an horizontal line for a certain x_0.
Let us also call (k_s^c, d_i) the point given by the intersection of this curve with the unstable 2-periodic branch. As for $k_s > k_s^c$ the orbit is attracted to the fixed point and for $k_s < k_s^c$ to the 2-periodic orbit with one saturated duty

cycle, a nonsmooth flip bifurcation is expected to occur for $k_s = k_s^c$ when numerically investigating the system as schematically shown in Figure 4.11(a).

However, let us expose here three important remarks.
On one hand, the curve $\zeta(x_0)$ is plotted in Figure 4.11(a) as an horizontal line just for explanatory reasons. In fact, some calculations show that $|\partial d_i/\partial k_s| \ll 1$, and therefore, for our propose here, we can consider $\zeta(x_0) = (k_s, d_i)$ with $d_i = ct$.
On the other hand, expecting a nonsmooth flip bifurcation implies that, for $v_{\text{ref}} \geq \tilde{v}_{\text{ref}}$ (above point B of Figure 4.7), both the period doubling and the corner collsion bifurcation curves should be numerically detected as the same curve, a nonsmooth period doubling bifurcation. However, numerical bifurcation curves in parameter space presented in [3] do not verify this condition. As we will see below, this is due to the use of numerical simulations possibly aggravated by the use of the linear approximation of the error surface.
Moreover, the location of the expected nonsmooth period doubling bifurcation curve should depend on which initial condition is used, as k_s^c depends on x_0. In Figure 4.11(b), the obtained results for two numerical simulations for $v_{\text{ref}} = 0.7$, using 1.000.000, 3.000.000 and 10.000.000 iterations are shown. It is well known that such a nonsmooth flip is not easy to detect numerically but, as it is shown in Figure 4.11(b), as the number of iterations increases, both bifurcations get closer so reminding a nonsmooth period doubling bifurcation as predicted. However, increasing arbitrarily the number of iterations, stable 2-periodic orbits between the period doubling and the corner collision are always found. For instance, Figure 4.11(c) shows the same numerical results using 20.000.000 iterations. As one can there observe, 2-periodic stable orbits are still being found between both bifurcations for such number of iterations, so the nonsmooth flip bifurcation seems to be not possible to detect just increasing the number of iterations. This fact is normally attributed to the slow dynamics near the bifurcation value, also called *critical slowing down effect*. However, we will give in next chapter another possible explanation to this fact based on the not exactly fulfillment of the ZAD condition.

On the other hand, we show in Figure 4.11(d) the obtained results when simulating the system numerically using two different initial conditions, one near the fixed point and another one near the saturated orbit. Assuming that the bifurcations there detected are nonsmooth flips, they are given for different values of k_s depending on which initial condition has been used as predicted.

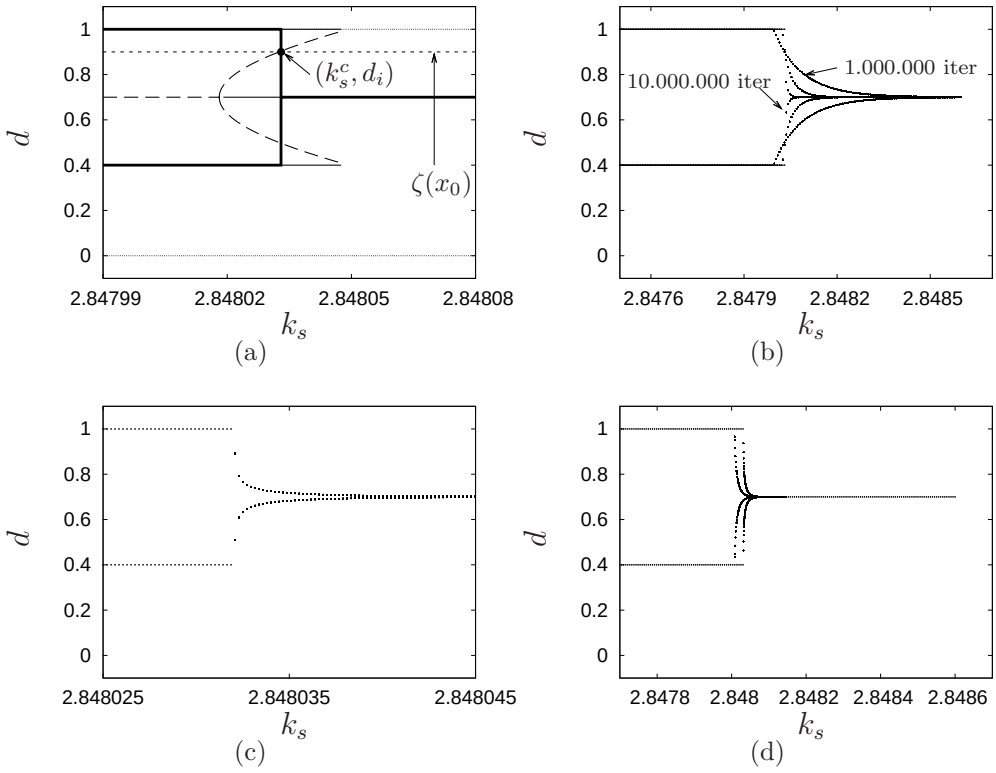

Figure 4.11: Simluations for $v_{\text{ref}} = 0.7$. (a) Expected numerical simulation. (b) Simulations with 1.000.000, 3.000.000 and 10.000.000 iterations. (c) Simulations with 20.000.000 iterations. (d) Simulations for two different initial conditions.

4.4.2 Numerical simulations for the supercritical flip bifurcation, $v_{\text{ref}} = 0.3$

From previous sections it is also clear that when trying to simulate the system for $v_{\text{ref}} = 0.3$, below point D of Figure 4.7, a supercritical flip bifurcation should be detected. As the non-saturated 2-periodic solutions are stable, one expects to find them numerically. In other words, the numerical one dimensional bifurcation diagram is expected to be similar to the one shown in Figure 4.10(h). However, as Figure 4.12(a) shows, even using so large number of iteration as 10.000.000 the shape of the 2-periodic stable orbits in that diagram is not exactly the expected one. Roughly speaking, the flip bifurcation is not produced in numerical simulations as a typical square root one but, on the contrary, both non-saturated 2-periodic branches seem to converge asymptotically to the fixed point as k_s increases instead of emerging

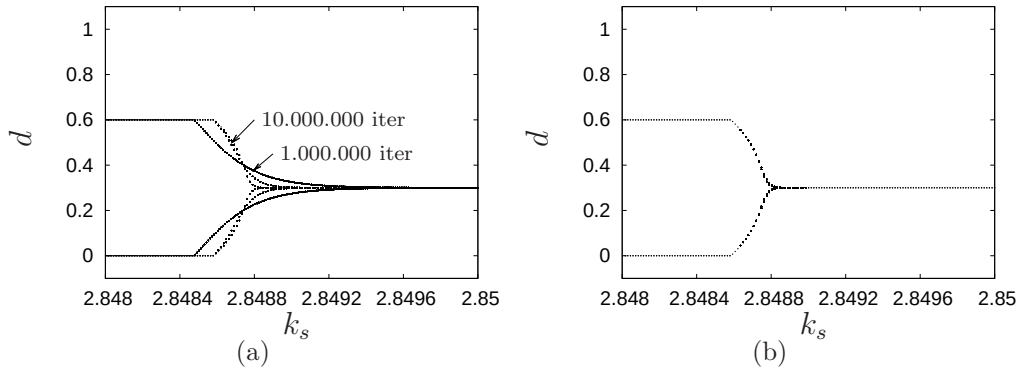

Figure 4.12: Simulations for $v_{\text{ref}} = 0.3$. (a) Simulations with 1.000.000, 3.000.000 and 10.000.000 iterations. (b) Simulations for two different initial conditions.

from this one.

On the other hand, as Figure 4.12(b) shows, the value of k_s where the period doubling bifurcation occurs does not change, as expected, using different initial conditions for the simulations as the 2-periodic branches are, in this case, stable and feasible.

As has been mentioned, all these differences detected between the analytical and numerical results can be justified using a critical slowing down argument. However, as we will show in next chapter, a similar effect is detected when introducing an small error on the ZAD condition arbitrarily different at each iteration of the Poincaré map.

Chapter 5

Perturbations on the ZAD condition

In this chapter we will give explanation, alternative to the critical slowing down effect, about what these differences between analytical and numerical results are due to.

As it was already explained, the origin of the detected differences between the numerical and analytical results can remain on the non-exact fulfillment of the ZAD condition. As 2-periodic orbits with one saturated duty cycle are clearly not fulfilling ZAD in the saturated iteration, it is of real interest to further analytically investigate these kind of orbits.

5.1 2-periodic orbits with one saturated duty cycle

In order to look for the existence of 2-periodic orbits with one saturated duty cycle and fulfilling the ZAD condition in the non-saturated iteration, that is, a $(1, d_2)$ $2T$-periodic orbits, we proceed as follows. Setting $d_1 = 1$ in equation (4.1) we first find the initial condition, $x^{**}_{0,1d_2}$, of a 2-periodic orbit with one saturated duty cycle on the first iteration. In order to make ZAD condition be fullfiled at the second one, we consider equation (4.3) using $d_1 = 1$. Now, varying d_2, we solve this equation for k_s so, for every $(1, d_2)$, the unique value of this parameter that makes ZAD be fulfilled at the second iteration is obtained.

In Figure 5.1 both duty cycles are shown. Notice that the straight line at $d \simeq 0.4$ concerning to the nonsaturated duty cycle is not horizontal and, therefore, there exists only one value for k_s, labeled as k_s^*, for which the ZAD condition is fulfilled in both iterations. This value corresponds to the

one given by the corner collision bifurcation curve just when $d_2 = 2v_{\text{ref}} - 1$, and, if $k_s \neq k_s^*$, the ZAD strategy is not fulfilled at the saturated iteration. We distinguish here two different cases: if $d_2 < 2v_{\text{ref}} - 1$, then $k_s < k_s^*$ and $\int_0^T s(t)dt < 0$, if $d_2 > 2v_{\text{ref}} - 1$, then $k_s > k_s^*$ and $\int_0^T s(t)dt > 0$.

On the other hand, let us do here the next remark. Recalling the results of section 4.3, 2-periodic orbits with one saturated duty cycle are not allowed to exist on the right hand side of the corner collision curve. However, in Figure 5.1 such orbits are plotted in that region (for $k_s > k_s^*$) although they do not contradict these above results as have been obtained forcing one duty cycle to be equal to 1. In the original system, where this condition is not imposed, all solutions are attracted to the fixed point.

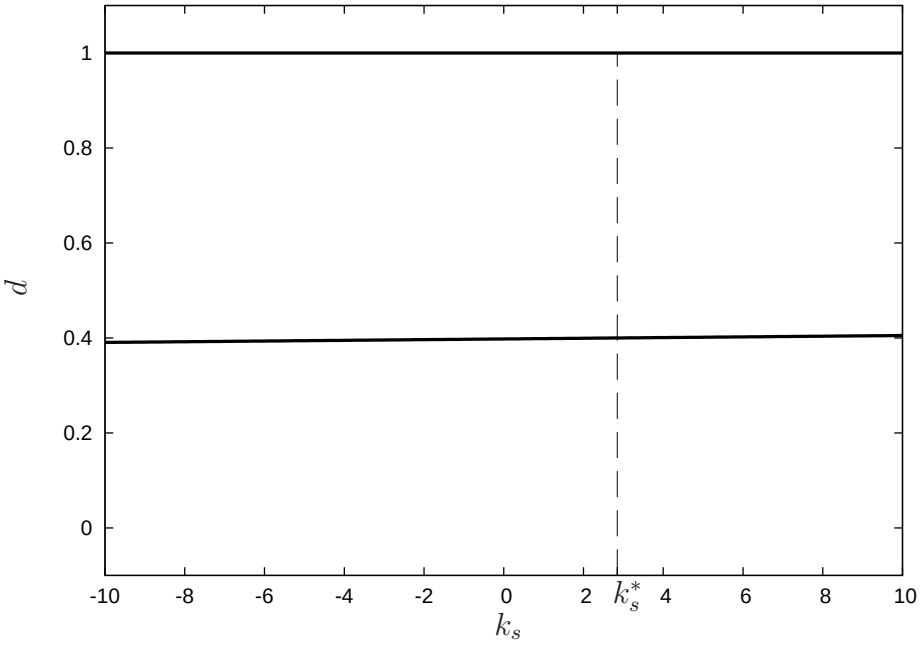

Figure 5.1: Duty cycles for a 2-periodic orbit with one saturated period. $v_{\text{ref}} = 0.7$, $d_1 = 1$ and $d_2 \in [3.9, 4.1]$.

5.2 ε-perturbing the ZAD condition

As a natural continuation of previous calculations, we find here 2-periodic orbits with non-saturated duty cycles almost fulfilling ZAD condition in one of both iterations. That is, (d_1, d_2) 2-periodic orbits such that ZAD is fulfilled

at the second iteration but almost at the first one. Therefore, let us introduce an ε-perturbation in the ZAD condition fulfillment in the whole $2T$ period, that is, let us replace equation (4.4) with

$$d_1 + d_2 + \varepsilon = 2v_{\text{ref}}. \tag{5.1}$$

We notice here that, if $\varepsilon > 0$, then $\int_0^{2T} s(t)dt < 0$ and, on the contrary, if $\varepsilon < 0$ then $\int_0^{2T} s(t)dt > 0$.
Next, we proceed as follows. Let first x^{**}_{0,d_1d_2} be the initial condition of a (d_1, d_2) 2-periodic orbit from expression (4.1). Let us also fix d_1 and set d_2 as given by equation (5.1). Then, let us solve for k_s equation (4.3). Finally, for every ε, varying d_1 and using preceding values for d_2 and k_s, we will find (d_1, d_2) $2T$-periodic orbits verifying ZAD condition at the second iteration but ε-closely at the first one.
Notice that, if $\varepsilon \neq 0$, the fixed point no longer exists as $d_1 = d_2 = v_{\text{ref}}$ is not a solution of equation (5.1). Therefore, when perturbing the ZAD condition on one iteration but not on the next one, the system no longer possesses any fixed point.

5.3 Bifurcations in the perturbed ZAD condition

Once this ε-perturbation is introduced in the ZAD condition, we notice that not only the fixed point is destroyed but also different structures of the dynamics of the system.
We present in Figure 5.2 several perturbed one dimensional bifurcation diagrams for a small range of ε using $v_{\text{ref}} = 0.7$. In this Figure $d > 1$ has been considered so also virtual orbits are plotted there in order to observe how this perturbation affects the (virtual) saddle node bifurcation.
Notice that there exists an $\varepsilon_0 < 0$ such that, $\forall \varepsilon \leq \varepsilon_0$, the (virtual) saddle node bifurcation no longer exists whereas it persists for $\varepsilon > 0$.

In Figure 5.3 we present the same situation for a larger range of ε together with the 2-periodic saturated solutions found in Figure 5.1. Notice that for $\varepsilon < 0$ the saturation of 2-periodic orbits is given on the right hand side of the corner collision bifurcation. Recalling the results of section 4.3 and the comments about Figure 5.1 presented in section 5.1, we now see that $(1, d_2)$ 2-periodic orbits are possible for the original system on the right hand side of the corner collision bifurcation curve if $\varepsilon < 0$.

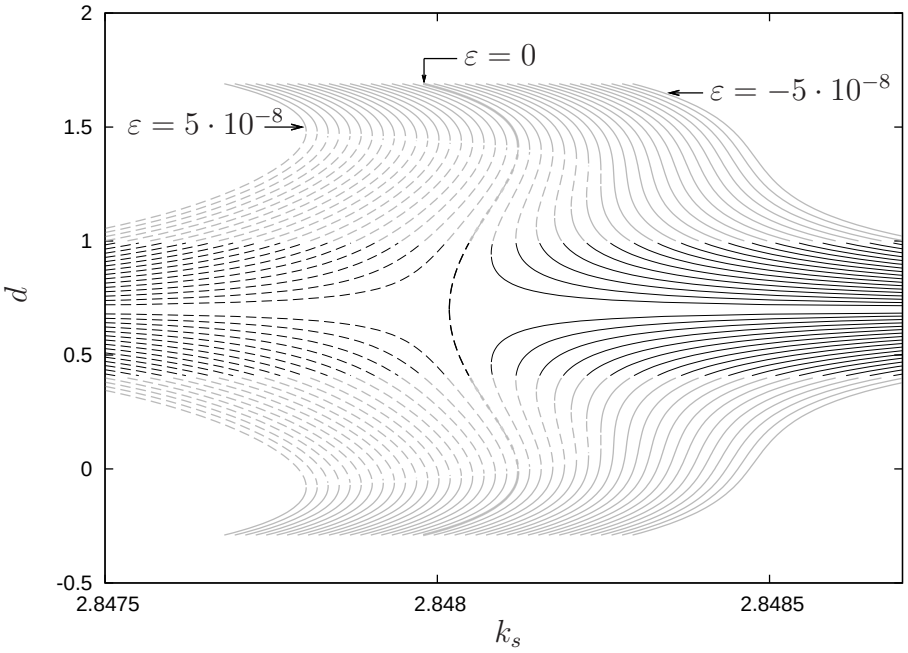

Figure 5.2: One dimensional bifurcation diagrams with an ε-perturbation in the ZAD condition in one iteration of 2-periodic orbits, $\varepsilon \in [-5 \cdot 10^{-8}, 5 \cdot 10^{-8}]$

Proceeding analogously for $v_{\text{ref}} = 0.3$, perturbed one dimensional bifurcation diagrams for the supercritical case are shown in Figure 5.4.

As perturbing the ZAD condition just in one iteration of a 2-periodic orbit is not a realistic situation, we also add such perturbation to the ZAD equation (4.3) in order to perturb the zero average condition in both periods. As one can observe in Figure 5.5, the results are almost the same as previous ones but for one lower order of ε. Notice that the scales of Figures 5.5 and 5.2 are exactly the same. However, results shown in Figure 5.5 have been obtained in shuch a manner that the perturbation has not been introduced equally at each iteration and, therefore, the fixed point remains not existing.

5.4 Implications on numerically solving the ZAD condition

As one can imagine, the bifurcation previously shown when perturbing the ZAD condition may have several implications when trying to simulate the

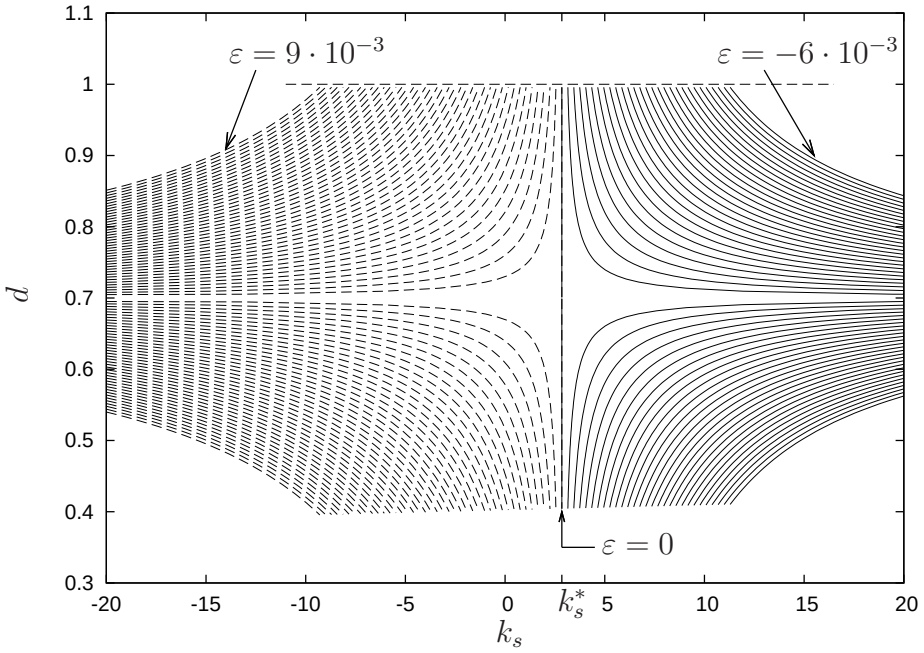

Figure 5.3: One dimensional bifurcation diagramas with an ε-perturbation in the ZAD condition in one iteration of 2-periodic orbits, $\varepsilon \in [-6 \cdot 10^{-3}, 9 \cdot 10^{-3}]$

system numerically. In order to present them in an accurate manner, let us first distinguish between values of v_{ref} which makes the saddle node bifurcation exist, even being virtual, and values for which this bifurcation does not. That is, values of v_{ref} above and below point B' of Figure 4.9.
Let us start first with the first ones region.

On one hand, the existence of $\varepsilon_0 < 0$ such that the saddle node bifurcation is destroyed $\forall \varepsilon \leq \varepsilon_0$ implies that the expected nonsmooth flip bifurcation presented in section 4.4.1 is not possible to find numerically if the error committed on the calculation of the duty cycle is not small enough, even increasing infinitely the number of iterations. However, there exists also an ε_1, $\varepsilon_0 < \varepsilon_1 < 0$, such that, $\forall \varepsilon \in (\varepsilon_0, \varepsilon_1]$, the whole unstable 2-periodic orbit is virtual. Therefore, $\forall \varepsilon \leq \varepsilon_1$, the nonsmooth flip bifurcation is not possible to detect numerically. In Figure 5.6(a) the expected numerical simulation for $\varepsilon = \varepsilon_1 \simeq -5 \cdot 10^{-9}$ together with the non-perturbed case $\varepsilon = 0$ for a certain initial condition d_i is shown.
On the other hand, as the fixed point is destroyed for $\varepsilon \neq 0$ even if the ZAD condition is perturbed at each iteration but not equally at each one, the nonsmooth period doubling is also not possible to reach numerically as , in fact, such a "doubling" has no sense in this case. However, for $0 > \varepsilon > \varepsilon_1$, there

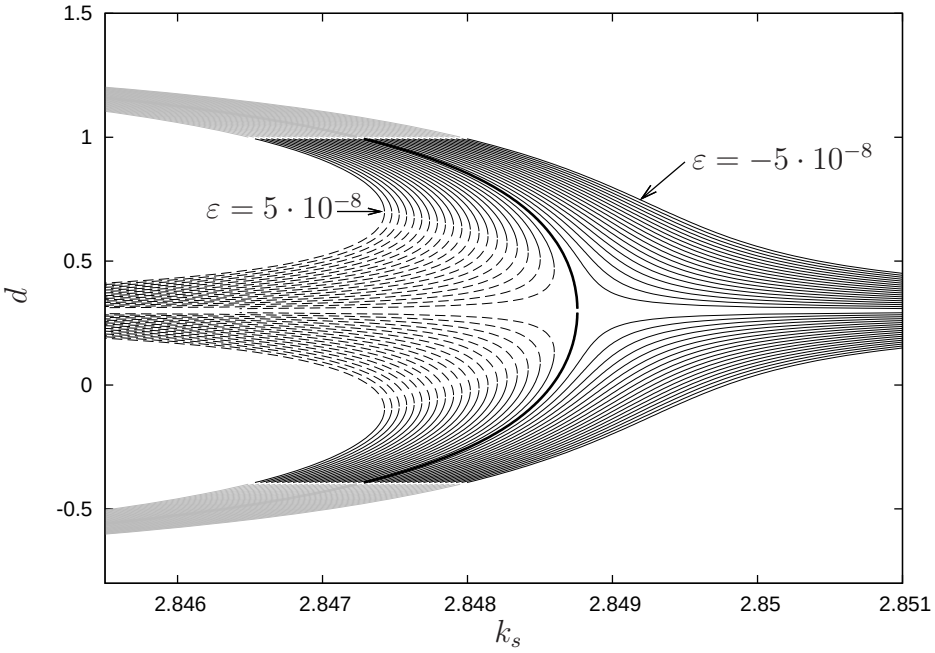

Figure 5.4: Perturbing the ZAD condition in one iteration on 2-periodic orbits, $\varepsilon \in [-5 \cdot 10^{-8}, 5 \cdot 10^{-8}]$. $v_{\text{ref}} = 0.3$

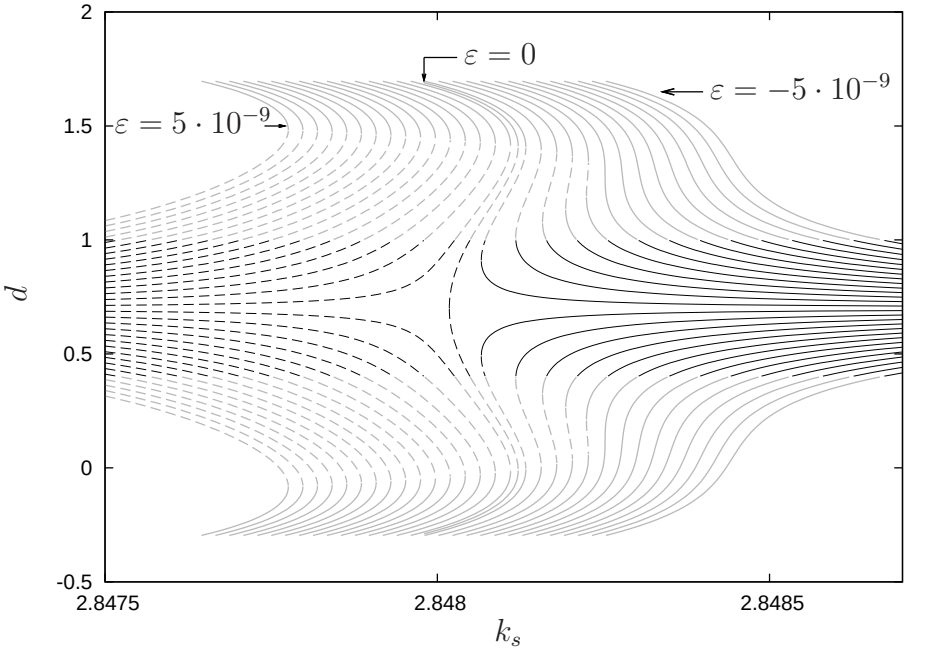

Figure 5.5: Perturbations in the ZAD condition in both iterations of 2-periodic orbits.

exist feasible-unstable 2-periodic orbits so a nonsmooth transition between the stable orbits to the saturated ones is expected to observe when numerically simulating the system. Figure 5.6(b) shows the expected numerical result for such an ε together with non-perturbed case. Notice that, in this case, also the nonsmooth transition to the saturation depends on the initial condition d_i given by the initial state variables used for simulating the system.

Concerning to the region below point B, notice that, in Figure 5.4, the shape of the 2-periodic branches for ε close to 0 are the same as the numerical obtained ones (see Figure 4.12(a)) as, for $\varepsilon < 0$, the 2-periodic branches are feasible and stable. As the fixed point no longer exists, we conclude that the typical square root shape of standard period doubling bifurcation is not possible to obtain completely when simulating the system numerically even increasing infinitely the number of iterations when the ZAD condition is not equally fulfilled at each iteration.

5.5 Implications on using the affine approximation of $s(t)$

As has been mentioned in previous chapters, the bifurcation curves in parameter space presented in [3] differ from the analytically obtained ones. Not only these first curves have been numerically obtained but also the linear approximation of the error surface, $s(t)$, has been used, while in the ones presented here and in [1], ZAD condition has been analytically imposed.
In [4], a comparison between the exact calculation of the duty cycle and the obtained by the affine approximation has been done. Taking into account that the advantages in computations presented by the use of such an approximation, the obtained error is more than acceptable. However, although this error is not there estimated, it is greater than 10^{-8} so, as Figure 5.5 shows, the saddle node structure is destroyed for such an order of ε. Therefore, the two-parameter bifurcations curves presented in [3] differ from the analytical ones as the destruction of the saddle node presented by the perturbation on the ZAD condition makes the period doubling remain on the right hand of the corner collision for all values of v_{ref}.

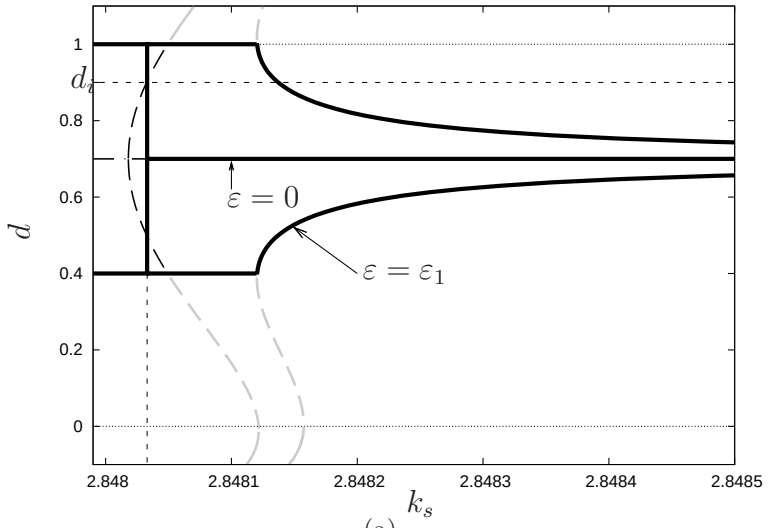

(a)

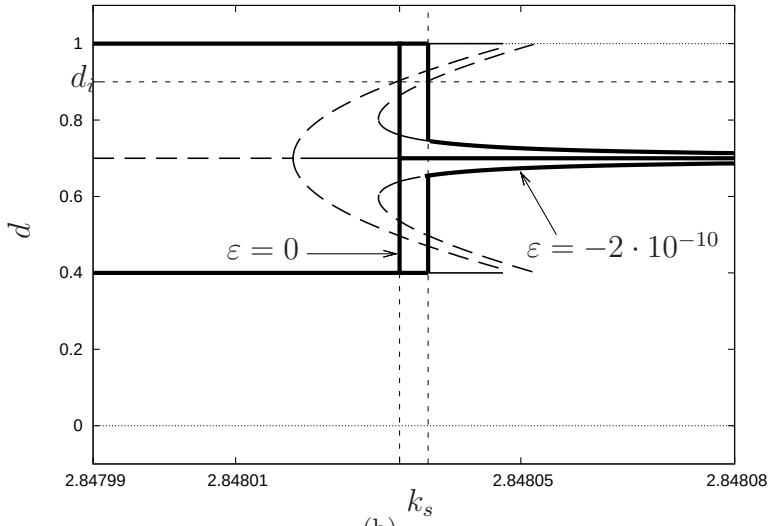

(b)

Figure 5.6: Expected numerical results for $v_{\text{ref}} = 0.7$. (a) $\varepsilon_1 = -5 \cdot 10^{-9}$ ($\simeq \varepsilon_1$). (b) $\varepsilon = -2 \cdot 10^{-10}$ ($\varepsilon_1 < \varepsilon < 0$).

Chapter 6

Conclusions

Considering virtual orbits we have shown that the transition between the subcritical and supercritical period doubling bifurcation is given by a saddle-node bifurcation that becomes feasible until it disappears at a new codimension two bifurcation point. Using this concept together with several one-dimensional bifurcation diagrams, we have also given a comprehensive explanation to other codimension two bifurcation points found in the references. Plotting the saddle-node bifurcation curve in the parameter space we have determined the regions of existence of all one and two-periodic objects including saturated orbits.

We have also proved that the whole structure of the parameter space is extremely sensitive to the exactly fulfillment of the ZAD condition, so checking this fact with numerical simulations. This sensitivity has permitted us to explain what the differences in the references are due to, although they can be attributed to a critical slowing down effect. Considering the first situation, we have shown that when working with the linear approximation, the error committed is big enough to destroy the saddle-node structure and, therefore, the period doubling curve remains always at the right hand side of the corner collision one.

Bibliography

[1] Fossas, E., Hogan, S.J., and Seara, T.M. "*Two-parameter bifurcation curves in power electronic converters*", IJBC, 2008

[2] Fossas, E., Griñó, R. and Biel D. "*Quasi-Sliding control based on pulse width modulation, zero average dynamics and the L_2 norm.*" In Proceedings VI International Workshop on Variable Structure Systems. 2000. pp. 335-344.

[3] Angulo, F., Olivar, F.G. and di Bernardo, M. "*Two-parameter Discontinuity-induced Bifurcation Curves in a ZAD-Strategy Controlled DC-DC Buck Converter*", IEEE Trans. Circ. & Sys. I, 2008, Vol. 55, pp. 2392-2401.

[4] Angulo, F. "*Análisis de la dinámica de convertidores electrónicos de potencia usando PWM basado en promediado cero de la dinámica del error (ZAD)*", Ph. D. Thesis, Universitat Politènica de Catalunya, 2004 (Spanish), available at http://www.tdx.cesca.es/TDX-0727104-095928.

[5] Di Bernardo, M., Budd, C.J., Champneys, A.R. and Kowalczyk, P. "*Bifurcations in piecewise-smooth dynamical systems: theory and applications*", Springer-Verlag: Berlin, 2007.

[6] Fossas, E. and Zinober, A. 2001 "*Adaptative tracking control of nonlinear power converters*". IFAC Workshop on Adaptation in Contronl and Signal Precessing. Connobio. Italy. pp. 264-266.

[7] Ramos, R., Biel, D., Fossas, E. and Guinjoan F. 2003 "*Fixed-frequency quasi-sliding control algorithm: application to power inverters design by means of FPGA implementation*". IEEE Trans. Power Electronics 18, 344-355.

[8] Bilalovic, F., Music, O., and Sabanovic, A. 1983 "*Buck converter regulator operating in the sliding mode.*" In Proceedings VII International PCI. pp. 331-340.

[9] Venkataramanan, R., Sabanovic, A., and Cuk S. 1985 "*Sliding mode control of DC-to-DC converters.*" In Proceedings IECON 1985. pp. 251-258.

[10] Carpita, M., Marchesoni, M., Oberti, M. and Puguisi, L. 1988 "*Power conditioning system using slide mode control.*" In Proceedings of the IEEE Power Electronics Specialist Conference. pp. 623-633.

[11] P. T. Krein, J. Bentsman, R.M. Bass i B. L.Lesieutre. "*On the Use ofAveraging for the Anallysis of Power Electronic Systems*". IEEE Transactions on power electronics. Vol. 5 no 2, 1990.